Stress-Strain Distribution in the Contact Surface of a Two-Layered RC Structural Element

Jozef SUMEC
Assoc. Professor
Fac. of Civil Eng.
Bratislava, Slovakia

Jozef Sumec, born 1945,
received his civil eng.
degree 1968, PhD degree 1975,
DSc degree 1990.

Norbert JENDZELOVSKY
Assoc. Professor
Fac. of Civil Eng.
Bratislava, Slovakia

Norbert Jendzelovsky, born 1958,
received his civil eng.
degree 1982, PhD degree 1981.

Summary

The contribution deals with the time-dependent analysis of the state of stress and strain distributions on the contact surface of a reinforced concrete two layered element (in the sense that „new material" means topping layer and „old material" means prestressed plate structure). We suppose that the structural system is linearly viscoelastic quasihomogenic isotropic continuum. The linear aging model for concrete creep is used. The theoretically derived solution procedures are examplified by particular numerical examples.

1. Mathematical Formulation of the Problem

We will deal in our analysis with the quasistatic problem of the two-layered planar composite structure with technologically conditioned defects. We suppose that the principles of the linear theory of viscoelasticity are valid. The mathematical representation of the discussed physical model is the operator equation [1]

$$L(u) = f \tag{1}$$

in the domain $\Omega = \Omega_1 \cup \Omega_2$ $(\Omega \subset E_3)$ which is bounded per partes smooth surface
$S = S_1 \cup S_2$ $(S_1 \cap S_2 = \varnothing)$, $u = u(P,t) = \{u(x,y,z,t), v(x,y,z,t), w(x,y,z,t)\}$ is a sufficiently smooth vector-function, where $P \in \Omega$, $t \geq 0$. The solution of the Eq.(1) satisfied the following conditions

$$u^{\lambda} = 0 \qquad\qquad \text{on } S^a, S^b \tag{2}$$

$$\sigma^{\lambda\kappa} n_{\kappa} + \sigma^{(0)\kappa\mu} n_{\kappa} u^{\lambda}{}_{,\mu} = \overline{F}^{\lambda} \qquad\qquad \text{on } S - \left(S^a \cup S^b\right), \tag{3}$$

$$u^{\lambda}\Big|_{\Omega_1} = u^{\lambda}\Big|_{\Omega_2} \qquad\qquad \text{on } \Omega_1 \cap \Omega_2. \tag{4}$$

This problem is equivalent to the problem of finding the element of energetic space which mininimalize energetical functional [1,2]

$$F(u) = (u,u)_{L(.)} - 2(u,f) \tag{5}$$

The basic idea of FEM is to represent the displacement functions $\mathbf{u} = (u, v, w)$ within the element by continuum shape functions of the form

$$u(x, y, z, t) = \sum_{i=1}^{L} N_i(x, y, z) u_i(t), \ldots \tag{6}$$

where N_i $(i = 1, 2, \ldots L)$ are the shape functions associated with the L nodes and
u_i $(i = 1, 2, \ldots L)$ are nodal values of the displacement $u(x, y, z, t)$, etc. The strain rate field within the element can be defined as [3]

$$\dot{\varepsilon}(x, y, z, t) = \mathbf{B}(x, y, z) \dot{\delta}(t), \tag{7}$$

where $\mathbf{B}$ is a matrix of gradients of the shape functions and $\dot{\delta}$ is the nodal velocity vector. The equilibrium of the stress rates $\dot{\sigma}$ is given by

$$\sum_{Ve} \int_{Ve} \mathbf{B}^T \dot{\sigma} \, dV = \dot{\mathbf{R}}^a, \tag{8}$$

where $\dot{\mathbf{R}}^a$ is the applied nodal load rate vector. The stress-strain relationship for inelastic rate processes may be given by the formula

$$\dot{\sigma} = \mathbf{D}(\dot{\varepsilon} - \dot{\eta}), \tag{9}$$

where $\mathbf{D}$ is elasticity matrix and $\dot{\eta}$ is the creep strain rate (for instance)

$$\dot{\eta} = \Re(\sigma, t, T).$$

We may transform the system of equilibrium equations into the matrix equation

$$\mathbf{K}\dot{\delta} = \dot{\mathbf{R}}^a + \dot{\mathbf{R}}^\eta \qquad \text{on } \Omega, \tag{10}$$

where $\mathbf{K} = \sum_e \int_{Ve} \mathbf{B}^T \mathbf{D} \mathbf{B} \, dV$ is the assembled stiffness matrix and

$$\dot{\mathbf{R}}^\eta = \sum_e \int_{V^e} \mathbf{B}^T \mathbf{D} \dot{\eta} \, dV \tag{11}$$

is the vector of the creep process. After some rearrangements Eqs (10) and (11) can be written in he incremental form over a time interval

$$\mathbf{K}\Delta\delta = \Delta\mathbf{R}^a + \Delta\mathbf{R}^\eta \qquad \text{on } \Omega, \tag{12}$$

where

$$\Delta\mathbf{R}^\eta = \sum_e \int_{V^e} \mathbf{B}^T \mathbf{D} \Delta\eta \, dV. \tag{13}$$

Numerical schemes for the solutions of Eqs (12), (13) are discussed in [4].

2. Linear Aging Concrete Creep and Shrinkage Model

The characteristic of concrete that distinguishes it from the traditional viscoelastic material is the aging effect. Experimental tests [5] indicate that response on the increment of load is independent of all other part load increments, so that the principle of superposition is valid. Due to this fact the integral-type creep law has the form [6]

$$\varepsilon(t) = \int_0^t \prod (t, t') d\sigma,$$ (14)

where

$$\prod (t,t') = J(t,t') \begin{bmatrix} 1 & -v & -v & & & \\ -v & 1 & -v & & & \\ -v & -v & 1 & & & \\ & & & \frac{1}{2}(1+v) & & \\ & & & & \frac{1}{2}(1+v) & \\ & & & & & \frac{1}{2}(1+v) \end{bmatrix}$$

and

$$J(t,t') = \frac{1}{E(t')} + \sum_{j=1}^{n} \hat{A}_j^{-1}(t')(1 - e^{-(t-t')/\tau_j}), \quad E(t') = E_{28}\sqrt{\frac{t}{4 + 0.85t}},$$

where τ_j are constants (retardation times) and $\hat{A}_j$ are aging coefficients. For shrinkage of concrete we can assume the relation [6]

$$\varepsilon_{sh}(t) = 0.0008c'(t - 7) / (35 + t - 7)$$ (15)

in which t is in days and drying is assumed to begin at $t_0 = 7$ days, $c' = \prod_1^6 c_i$ is correction factor [6].

3. Numerical Example

This section deals with the numerical solution of some viscoelastic aging creep problems - two layered reinforced concrete plate with a prestressed lower layer. The analysed plate is simply supported in positions a and b (Fig. 2). The length of the system is 6000 mm, width 1190 mm. The thickness of the lower layer is 70 mm and upper concrete layer 170 mm, respectively. The cross-section of the given structure is in Fig.1
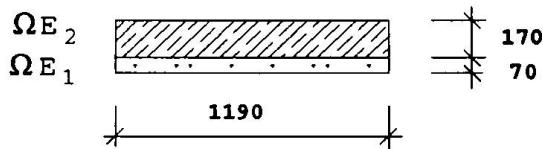

Fig. 1 Cross-section of the plate system

The plate carries a uniformly distributed load with the intensity $q = 5{,}68$ kN / m^2 (dead load) and a line load with the intensity $p = 20{,}07$ kN/m (Fig.2). The triangle represents the course of the prestressed force in the individual strings. The prestress on 8 wires ϕ 5mm is realised.
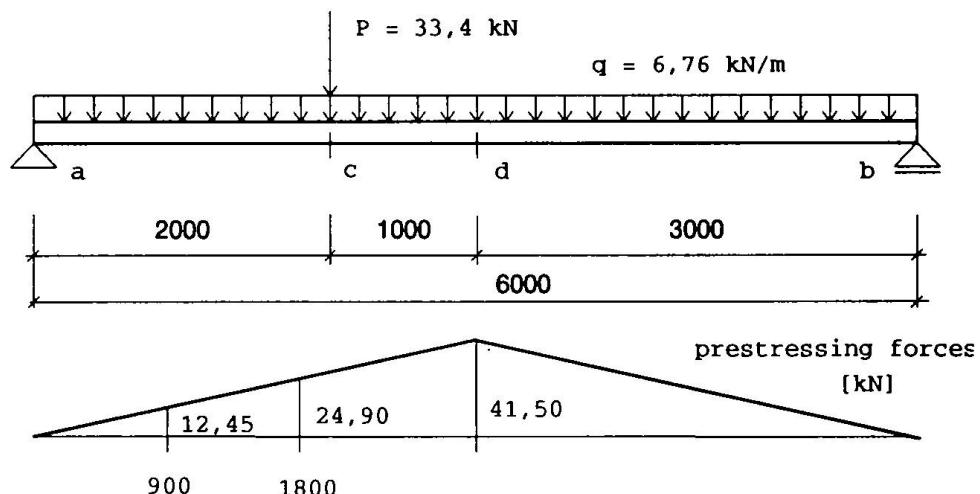
Fig. 2 Longitudinal section and values of prestressed forces

Characteristics of the materials are as follows: a lower concrete layer of type B 30 ($E_1 = 32500$ MPa) according to the code STN 73 1201 [7] and an upper layer B 20 ($E_2 = 27000$ MPa), respectively. The following cases were considered:

1) upper layer shrinking, lower layer non creeping ☐ s/nc
2) both layers creeping   O c/c

The time intervals taken: 0, 5, 10, 20, 50, 100, 300, 500, 1000 and 3000 days. We assume a 28 day time interval for hardening of concrete. The top layer was laid down after 200 days. Between the layers the conditional technological horizontal defect range of the half-span was taken into account , too (case B). It means, that the following cases were solved:

A - without defect on section a - b
B - with defect on the section a - d.

Figs 3 and 4 represent the time - dependet vertical deflections in the half-span of the system.
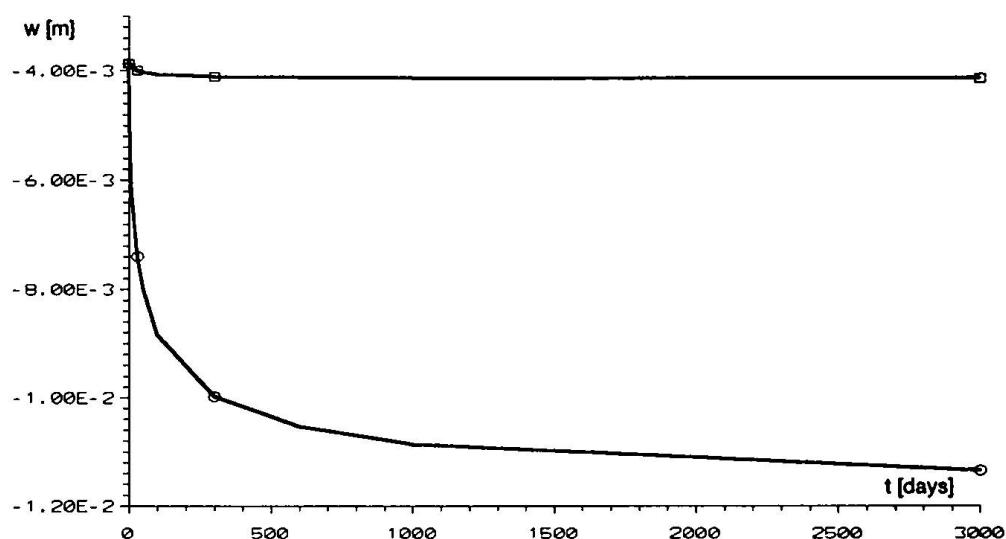
Fig. 3 Vertical deflections w(d,t) for case A, ☐ s/nc, O c/c
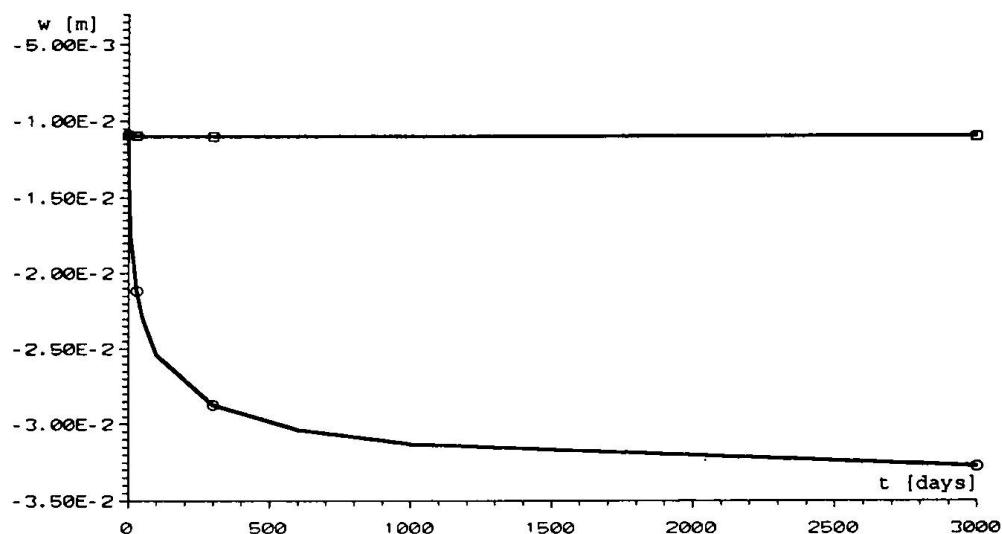
Fig. 4 Vertical deflections w(d,t) for case B, □ s/nc, O c/c

Normal and shear stresses for individual cases (A and B) under line - load (position c - where max. bending moment was expected) were calculated. Courses of normal stresses σ_x for cases A and B are given in Figs 5 and 6.
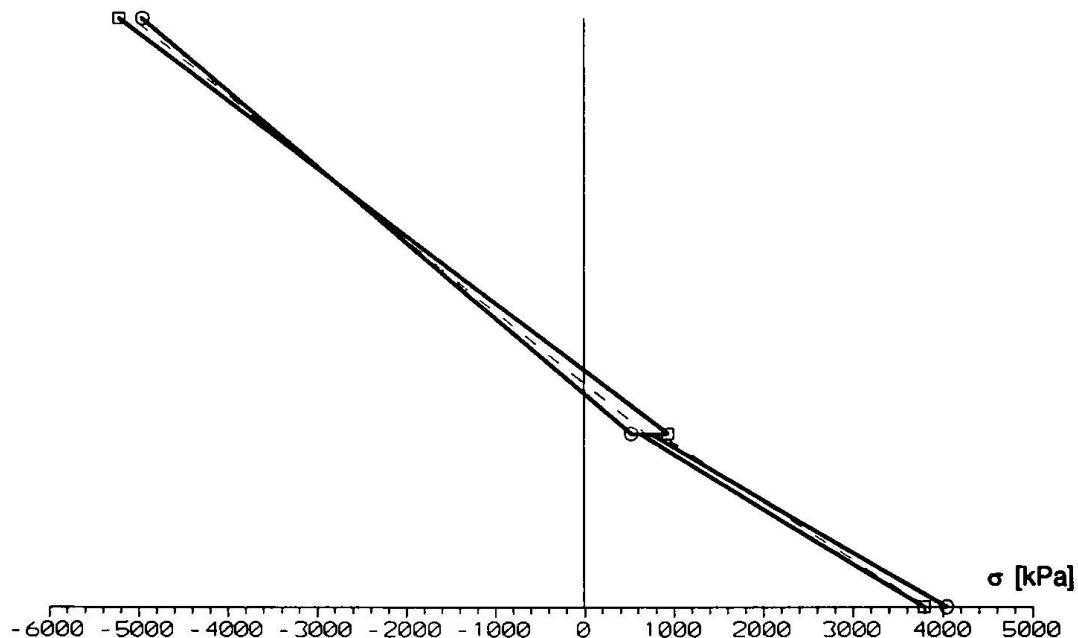
Fig. 5 Normal stresses $\sigma_x(c,t)$ for case A; □ s/nc, O c/c. The full lines represent values

$\sigma_x(c,t \rightarrow \infty)$ and dashed line $\sigma_x(c,t \equiv 0)$
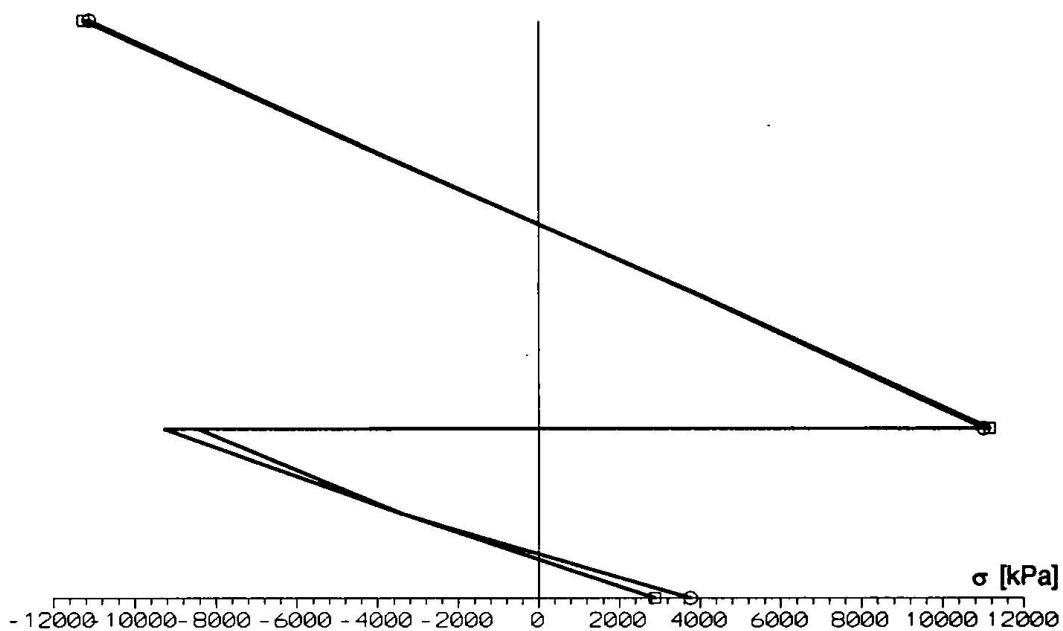
Fig. 6 Normal stresses $\sigma_x(c,t)$ for case B; □ s/nc, O c/c. The full lines represent values $\sigma_x(c, t \rightarrow \infty)$ and dashed line $\sigma_x(c, t \equiv 0)$

4. Conclusions

- on the interface of the layers cumulation of the shear stresses on the perimeter of the structure occured
- creep - deflection was 3 time larger than classical elastic deflection, that positively influence the course of the stresses
- the presence of technologically conditioned defects on the interface of the layers negatively influenced the stiffness of the system, in spite of the prestress on the lower layer
- a very significant element of the layered system is the technological surfacing, of the interface of the layers.

References

1. Mikchlin, S. G.: Variational Methods in Mathematical Physics (in Russian), Nauka, Moscow 1970.
2. Washizu, K.: Variational Methods in Elasticity and Plasticity. 3rd Ed., Pergamon Press, N.Y., Oxford, Tokyo, 1982.
3. Zienkiewicz, O.C.: The Finite Element Method. 3rd Ed. McGraw-Hill, N.Y., 1977
4. Wiliam, K.J.: Numerical solution of inelastic rate processes. Comp. & Struct., 8,1978, pp. 511-531.
5. Sumec, J.: Mathematical modelling of materials with time-dependent physical properties (in Slovak). Internal Research Report III-3-4/9.4, USTARCH SAV, Bratislava 1983
6. Bažant, Z.P.: Theory of creep and shrinkage in concrete structures: a precis of recent developments. Mech. Today,2, 1975, pp 1-93.
7.STN 73 1201. Design of concrete structures.

Performance and Stud Failure in Steel-Concrete Composite Beams

Jan L. VITEK
Assoc. Professor
Czech Technical Univ.
Prague, Czech Rep.

Jan L. Vitek, born 1957,
received his PhD. Degree
from the CTU in Prague
in 1985. His field of
interest are prestressed
concrete and concrete
structures, numerical
methods and failure analysis.

Vladimir KRISTEK
Professor
Czech Technical Univ.
Prague, Czech Rep.

Vladimir Kristek, born
1938, received his PhD.
Degree in 1967 and his DSc.
Degree in 1977 from the
CTU in Prague. Presently
head of Department of
Concrete Structures and
Bridges.
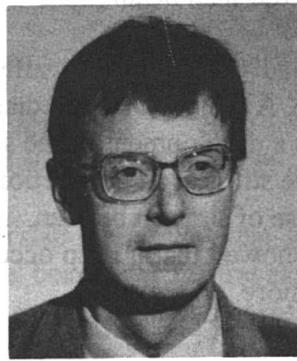
Summary

The effect of deformability of connection in composite beams was investigated on the basis of an experimental research. The performance was studied in both ultimate and serviceability conditions. The differences in performance between bridge and flooring composite beams are shown. The use of composite construction to improve buckling resistance and to reduce shear lag effects in box girders is proposed.

1. Introduction

Concrete steel composite structures are very efficient. Concrete is effective in compression and steel in tension, compressed steel parts are stiffened against buckling by a concrete slab. In old composite structures, a very stiff connection between steel and concrete was designed. Welded studs are connectors which are used very often mainly because of the simple production. The studs are flexible to some extent and therefore only partial interaction between a steel flange and a concrete slab exists. This implies that slip occurs at the interface, and so causes a discontinuity of strains. For most connectors used in practice, failure by vertical separation is unlikely and any uplift would have only negligible effect on the behaviour of the composite structure. If the deformability is taken into account in the design, the steel concrete structures can perform satisfactorily during their whole service life.

2. Stud resistance

A series of experiments has been carried out at the CTU Prague, in order to get the load slip diagrams, which made it possible to observe the progressive failure of one stud. They were arranged so that the results were not influenced by redistribution of the load between the two studs as it is in the case of a usual push out test. The loading process was controled by slip between steel and concrete which made it possible to detect the drop of ultimate load after failure. The mode of failure depends on the length of the stud embedded in concrete slab, on the diameter

of the shank of the stud and on the quality of concrete. It may be simply concluded that the short studs fail due to failure of concrete adjacent the stud and longer studs, which are well anchored in concrete usually fail by reaching the ultimate load carrying capacity of the shank in shear just above the steel beam.

The load - slip diagram is affected by the failure mode of the stud at the final stage just before its failure. A typical load-slip diagram of one stud is plotted in Fig. 1. The initial stage of the diagram shows a development of the shear force without any relevant slip. Then the slip starts to develop and the stiffness of connection is reduced significantly. Before failure of the stud a considerable increase of slip can be seen. Results of the experimental study carried out at studs of different sizes showed that no slip occurs if the shear force is about 25-30% of the ultimate shear force or even more.

Stud 16/60 mm
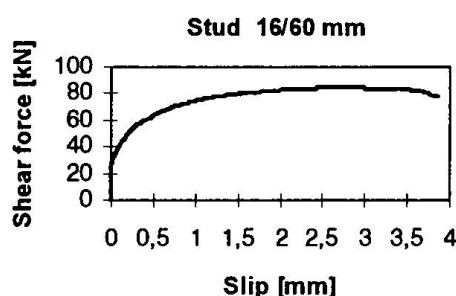
Fig. 1 Shear - slip diagram of one stud tested

3. Modelling of the stud performance in ultimate limit state

In the ultimate limit state of steel concrete composite beams, the failure may be achieved in various modes. (i) The stress in steel exceeds the yield limit, (ii) the stress in concrete exceeds strength in concrete or (iii) shear force in contact between concrete and steel exceeds the load carrying capacity of the connection. The last case need not necessarily lead to colaps of composite beams, however, a significant redistribution of internal forces can result due to failure of steel or concrete earlier than it would be expected assuming a stiff connection between steel and concrete.

To model failure of connection between steel and concrete, a simplified method has been developed [2]. The performance of studs is assumed according to a quadrilinear diagram (Fig.2). The first two lines (ascending part of the diagram) can be determined from the experimental results directly. The descending branch can be taken also from deformation controlled tests and the last horizontal line represents friction between steel and concrete after failure of studs. If no experiments are available, the descending branch can be assumed according to an empirical calculation, e.g. [1].

The behaviour of composite beams depends on the geometry of the cross-section. The beams used in buildings have rather thick and wide concrete slabs compared with the steel beam dimensions. The neutral axis usually lies in the concrete slab. Thus, a part of concrete section is under tension, which causes cracking and reduces stiffness of the slab. The studs are anchored in the tensile zone, and so their stiffness is necessarily lower than that of the studs anchored in concrete under compression. The contribution of the slab to the overall stiffness is high and the structure is sensitive to cracking, creep and shrinkage effects.
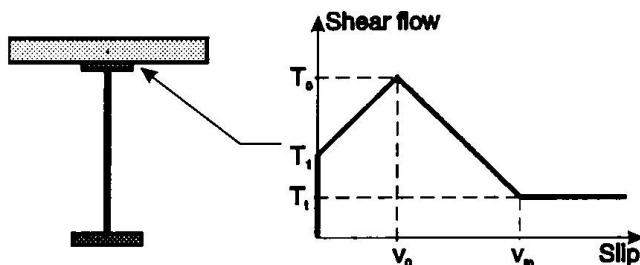
Fig. 2 The cross-section of composite beams studied and the idealized shear - slip diagram

Bridge beams behave differently. They are rather deep and the concrete slab is relatively thin. The width of the concrete slab is comparable with the dimensions of the steel beam. The neutral axis lies normally in the steel part of the cross section and thus the concrete slab is fully in compression zone. The studs are anchored in the compression zone of the slab which increases their load carrying capacity.

The distributions of the bending moments and axial forces in composite beams with deformable and stiff connectors are different. Near midspan, where the connection is stiff, the total bending moment is taken by the axial forces in steel and concrete, which form a couple. On the other hand, at the end regions of the beam, the connection can be rather weak due to partial failure of connectors, and then the total bending moment equals roughly the sum of the moments in the cross-section parts, with a reduced contribution of the couple of axial forces. Typical stress distributions in the concrete slab and in the steel beam of a bridge composite beam are plotted in Fig.3a,b together with the shear flow variation (Fig.3c) along the bridge span of the length 30 m. The stress variations are plotted in the stage when the connection partialy failed and the stress in the steel beam reached the stress limit. The sudden changes in the stress variations are due to a simplified shape of the shear force - slip diagram as shown in Fig.2. In a real structure, the changes would be smooth, but not disappear. In the central part, where no slip occurs, the stress becomes lower and in the end parts the slip develops. The extreme compression stress in concrete is in the central part, the extreme tensile stress at the bottom surface of the concrete slab develops approximately in the middle of the end parts (Fig.3a). The extreme stresses in steel are at the location where the slip starts to develop (Fig.3b). In the case of stiff connection, the stresses would correspond to those stresses plotted in Fig.3 at the central part of the beam and the stresses in steel (particularly in the top flange) would be significantly underestimated against the real arrangement with deformable connection. Tensile stresses occur at the bottom surface of the concrete slab (Fig.3a) where compression stresses in concrete would be expected in the case of stiff connection.

4. Perfomance in the serviceability limit state

The effect of variable stiffness of connection has been studied on a bridge beam of 35 m span. The depth of the steel I beam was 2.84 m and the thickness of the 2.125 m wide concrete slab was 0.2 m. The deformability of connection significantly affects the stress distribution and deflections of composite beams. However, its effect on stress and deflection variations is not proportional with respect to the deformability of connection. The degree of deformability varies from 0 (stiff connection) to 1 (no connection) in this study. The bridge beam with deformable connection exhibits a deflection w_{def} and the bridge beam with stiff connection has a deflection w_{stiff}. The
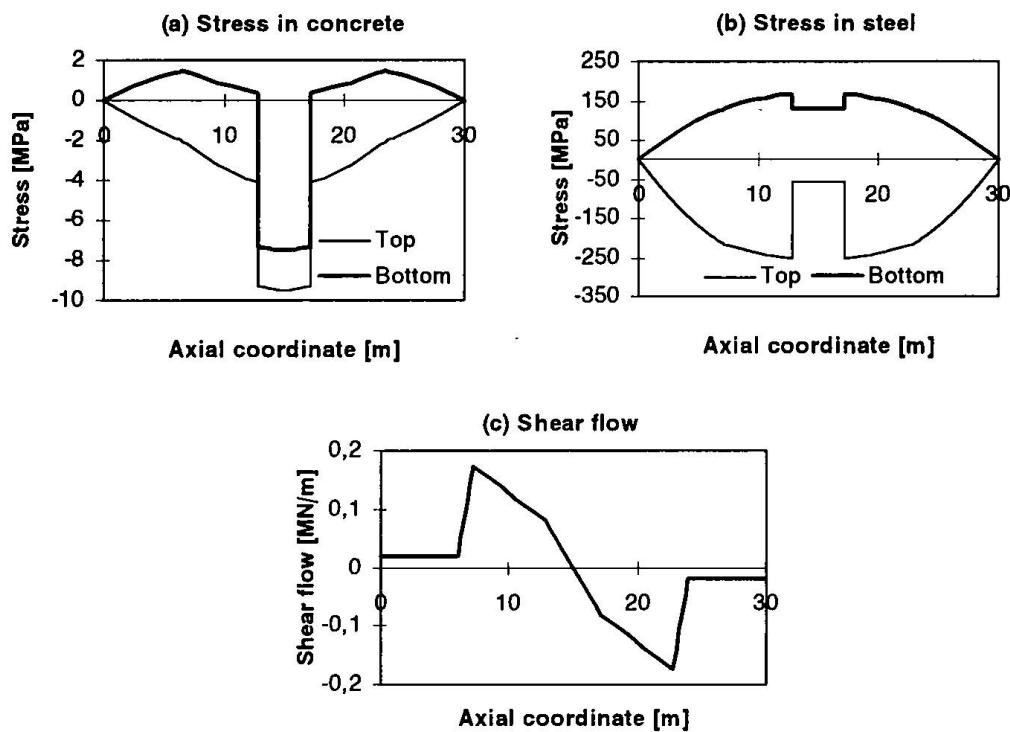
Fig. 3 Stress distributions and shear flow variation along the length of the beam

ratio w_{def}/w_{stiff} in dependence on the deformability of connection is plotted in Fig.4a. The thin line illustrates the effect of short term loading (age of concrete 28 days). It can be seen that the increasing connection deformability has initialy low effect on the deflection ratio, in the middle part of the diagram a substantial increase of deflection takes place and in the right hand side part of the diagram again very small change is seen. The thick line (10000 days after loading) shows increase of deflection ratio due to long-term loading. At the beam with stiff connection the effect of creep of concrete is significant, because of a great contribution of concrete slab to the overall bending moment, due to action of axial forces. At the beam with very deformable connection, the contribution of concrete slab to the overall bending is small, because the flexural stiffness of the concrete slab is much smaller than the stiffness of the steel beam. Therefore the creep effect is negligible. The development of stress redistribution in steel exhibits a similar trends like deflections.

The behaviour of the bridge beams was compared with the behaviour of the flooring beam. The depth of the rolled steel I beam was 312 mm, the concrete slab was 120 mm thick and 2.5 m wide. The deflection ratio similar to that of the bridge beam in dependence on the deformability of connection is plotted in Fig. 4b. The thin line (short term loading at the age of concrete 28 days) shows a similar trend as that of the bridge beam, however, the increase of deflection is higher (bridge beam 1.75, flooring beam 2.5). If the long-term load is assumed (thick line - 10000 days), the increase of deflection is even more significant. The concrete slab represents a significant part of the cross-section and its stiffness, which is reduced due to creep, influences significantly the deflection of the whole composite beam. Flooring beams are therefore more sensitive to the creep than bridge beams. The redistribution of stresses is also more significant at floor composite beams than at bridge composite beams.
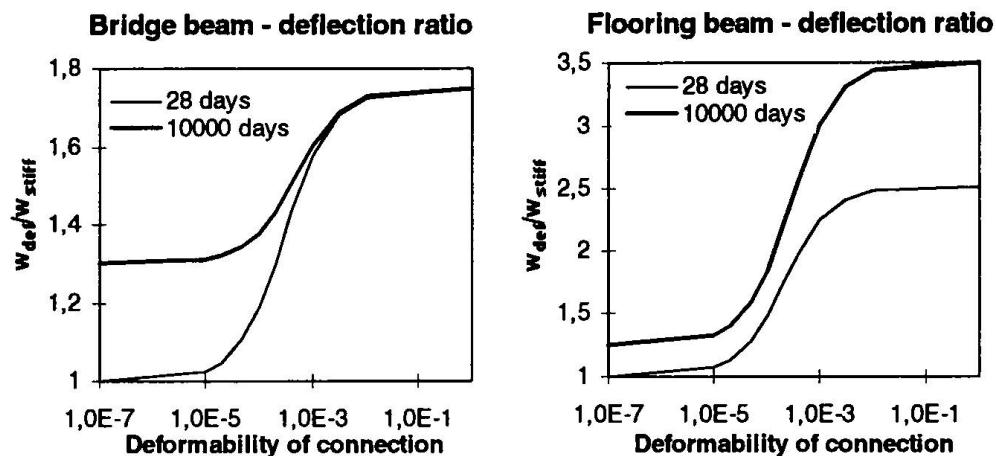
Fig. 4 Deflection ratio of the beams with deformable and stiff connection

5. Buckling resistance and controlling the effect of shear lag in box girders

The composite action may also be very effectively applied to increase the buckling resistance in the bottom flange plates in the hogging moment regions over the internal supports of continuous girders which are simultaneously very suspectible to the effect of shear lag.

It is well known that the effects of shear lag are particularly severe in local regions immediately adjanced to applied concentrated loads, in flange plates that are wide in relation to their length and in flanges that are longitudinally stiffened. In the case of a continuous steel bridge girder, these three circumstances can coincide to produce an exceptionally high shear lag effect in the lower flange over an intermediate support. Bridge bearings are often positioned under girder webs and bear almost directly on to the girder. The points of contraflexure are usually close to the intermediate support so that the effective span of the girder is short and the resulting span/width ratio is well within the critical range. Within such a region of hogging moment, the lower steel flange may be heavily stiffened against buckling under longitudinal compression.

A substantial reduction in the accentuated shear lag effect due to longitudinal stiffening is possible. The flange plate within the critical region can be stiffened with a layer of concrete that is made to act compositely with the steel flange which will be easy to place on the lower flange of the box over the intermediate support.

As an example a multispan, continuous bridge girder is considered and the performance of the two types of cross-section shown in Figs 5(a) and 5(b) is compared. In the first case, both flanges of the steel girder are stiffened by longitudinal ribs in the conventional way, with the lower compression flange stiffened by nine ribs to give a ratio of stiffener/flange plate area of 0.2. At an internal support, the distance between points of contraflexure is calculated to be 15.2 m so that the flange span/width ratio is 2.2. The girder is subjected to uniform line loading of 100 kN/m above each web and the upward reaction force at the support is calculated as 3600 kN; this is distributed over a bearing length of 100 mm.The distribution of the longitudinal stress across the width of the bottom flange above the intermediate support is plotted in Fig 5(a). It shows the expected shear lag effect with the amplified edge stress reaching a maximum value of 147.2 N/mm^2. The alternative solution is shown in Fig. 5(b). In this case, the thickness of the lower flange has been reduced from 12 mm to 8 mm and the lower flange stiffeners have been removed
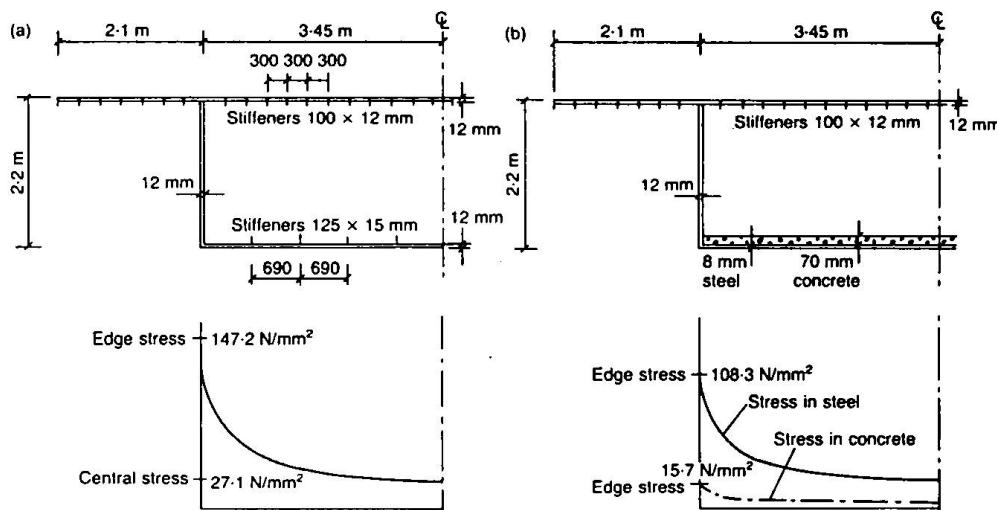
Fig. 5   Stress in an typical bridge girder. (a) Stiffened bottom flange, (b) Composite bot. flange

and replaced by a 70 mm thick layer of concrete acting compositely with the steel; other girder details remain the same. The plotted values show a significant reduction in the maximum steel stress from 147.2 N/mm^2 to 108.3N/mm^2. This reduction of about 27%, together with the amount of steel saved, shows the effectiveness of the proposed method.

Changing the number, flexibility, spacing and distribution of studs it is possible to control the distribution of axial stresses in the steel flange and in the concrete layer. It is obvious that as the stud stiffness increases the steel sheds more of its load into the concrete. On the other hand, to achieve the buckling resistance the use of a reduced number of studs can be sufficient.

6. Conclusions

1. Studs of different sizes were tested until failure and the shear force - slip diagrams were investigated. The slip has a significant effect on the distribution of internal forces, if the connection starts to fail. In those regions where slip occurs, the overall bending is transfered more by local bending of the steel beam and of the concrete slab. In the case of the simply supported beam subjected to a uniformly distributed load, the extreme stress in steel beam need not be at the midspan.

2. The effect of deformability of connection concerning the redistribution of stress and the growth of deflections, both due to short and long term loadings, is much more pronounced at flooring composite beams than that at the bridge composite beams.

3. Composite construction can be efficiently applied to achieve required buckling resistance and to control the effect of shear lag in box girders.

References

[1] Bažant, Z.P., Vítek, J.L.: *Stud Connectors in Comoposite Beams: Simplified Failure Modleing and Size Effect.* in Fracture and Damage of Quasibrittle Structures, Bažant et al. eds. E & FN Spon, London, 331-341

[2] Bažant, Z.P., Vítek, J.L.: *Composite Beams with Deformable Connection: Damage and Size Effect.* Submitted for publication, Journal of Struct. Eng., ASCE.

[3] Evans, H.R., Křístek, V. and Škaloud, M.: *Strengthening steel box girder bridges by controlling the effects of shear lag,* Proc.Instn Civ. Engrs Structs and Bldgs, Paper 10593, Nov. 1994, **104**, pp. 483-488

Study of Shear Bond in Steel Composite Slabs

Jacques RONDAL
Professor
University of Liège
Liège, Belgium

Jacques Rondal, born 1944 in
Noiseux (Belgium), received his
civil engineering degree and his
doctoral degree from the
University of Liège (Belgium).
He is currently Professor of Civil
Engineering and is the author of
several books and more than 200
scientific papers.

Alkistis MOUTAFIDOU
Civil Engineer
University of Liège
Liège, Belgium

Alkistis Moutafidou, born 1965 in
Thessaloniki (Greece), received
her civil engineering degree from
the Aristotle University of
Thessaloniki (Greece) (1988), is
working on her doctoral thesis
entitled "Study of shear bond in
steel composite slabs" at the
University of Liège (Belgium).

Summary

The aim of this paper (which consists a part of the doctoral thesis of the second author) is to study the collaboration (and especially the role of the embossments to the shear bonding) between the cold-formed profiled sheeting and the concrete in a composite slab. In order to attempt this aim, an experimental program has been undertaken on shear bond pull-out tests and a numerical model, with the help of a non-linear 3D finite element program, using large strains, has been developped to simulate the shear bond between the two materials.

1. Composite slabs

1.1 General

A composite slab consists of a cold-formed profiled steel sheet covered with a concrete (containing or not reinforcement). Such slabs, which incorporate profiled steel sheeting as both permanent formwork and tensile reinforcement of an in situ concrete slab and through deck welded shear studs to provide composite beam action, are becoming a very popular form of flooring system in a lot of countries. This success is due to the significant constuction benefits occuring as well as provision of an elegant structure.

There are many types of profiled sheets used for the construction of composite slabs, which vary, for exemple, in form, rib depth, by the methods of stiffenning the flat elements of the profil etc.

The bond between the concrete slab and the profiled sheet must be able to transmit longitudinal shear at the steel-concrete interface. This connection can be made, for exemple, by embossments, by the re-entrant shapes of the ribs creating a bond by friction or by other ways.

1.2 Types of shear bonding between cold-formed steel sheeting and concrete

Three types of shear bonding between cold-formed steel sheeting and concrete have been observed:
(a) *chemical bond* (bond resulting from the adherence of the cement paste to the steel sheeting; such bonds are broken under impact or repeated loading); (b) *frictional resistance* (resistance to applied shear forces, proportional to the application of lateral force between the steel sheeting and the concrete); (c) *mechanical resistance* (the physical interlocking of concrete and steel sheeting; such physical interlock occurs at abrupt changes in geometry such as embossments)[1].

Frictional and mechanical resistances are in reality due to the same phenomenon. They differ only in scale: frictional resistance is related to microscopic variations in surface geometry i.e. roughness; mechanical resistance is related to macroscopic geomettic differences i.e. embossments[1].

1.3 Composite slab behaviour

Learning upon test observations, three failure modes were established as follows: (a) *vertical shear* (or punching failure near concentrated or line loads; this is associated with heavy wheel loads or short span lengths); (b) *shear debonding* (resulting in the loss of composite action; loss of full composite action is indicated by the initiation of end slip); (c)*bending* (due to plastification of sheeting or crushing of concrete; normally, partial or complete plastification is observed after the loss of full composite action for long spans)[1].

2. Shear bond pull-out test for cold-formed steel composite slabs

2.1 General

A shear bond test is used to determine the nature of composite action between two materials; so, the shear bond pull-out test is used to predict the full-scale behaviour of cold-formed steel composite slabs (Fig. 1).

The experimental results help us to a better understanding of the failure procedure, of the shear-lateral force behaviour and of the shear-slip behaviour. For more informations about the pull-out test,like the test design (composite slab behaviour, modelling considerations), the experimental investigation (specimen geometry, materials, test frame, preparation of the specimens and test procedure) *Fig.1 Pull-out test[1]* and so on, see [1].

Fig.1 Pull-out test[1]

An experimental program has been undertaken at the M.S.M. Laboratory on shear bond pull-out tests; different types of cold-formed steel sheeting have been used, but we chose to work only with one of them, the profiled sheeting of type Hibond 77 (Fig. 2).

The results of a pull-out test are resumed to a (P-u) curve (where P is the shear load and u is the
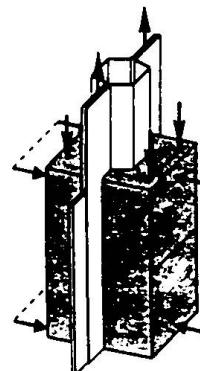
average slip). The curves (P-u) for the Hibond 77 (M.S.M. Lagoratory) are presented in Fig. 3.
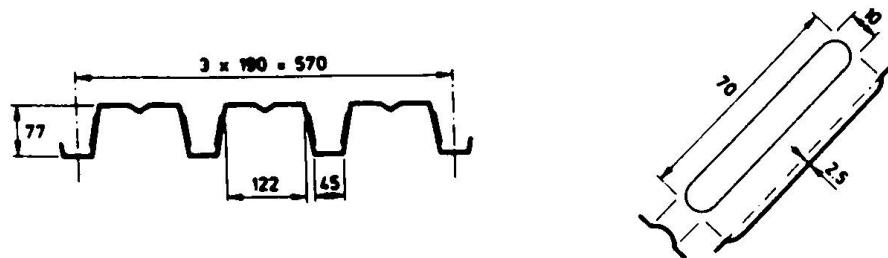
Fig. 2 Cross section and embossment pattern of Hibond 77 (all dimensions in mm)
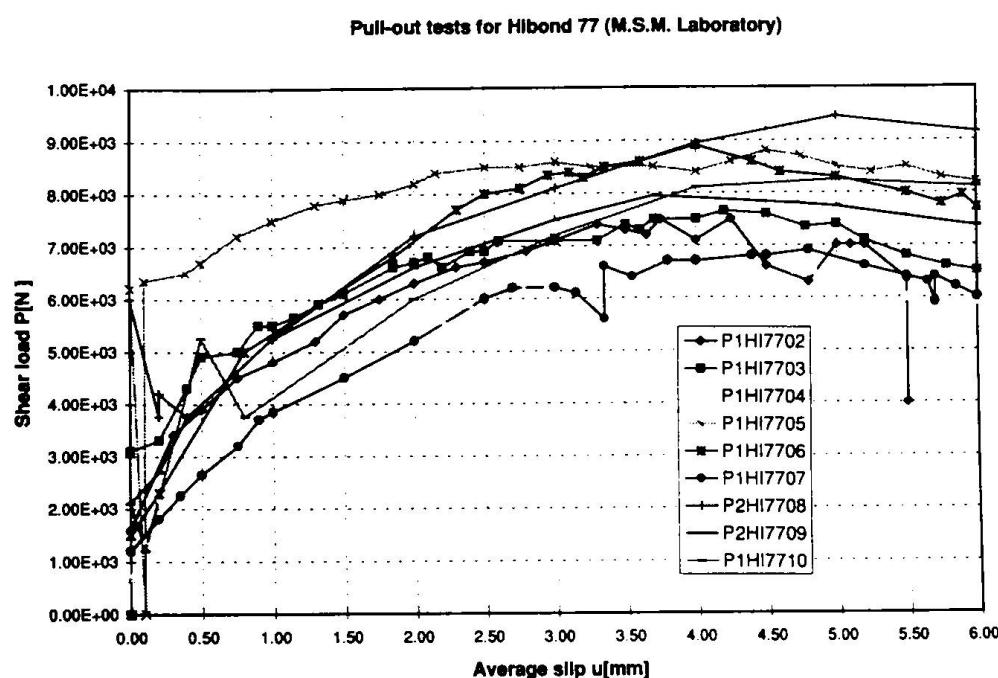
Fig 3 Shear-slip (P-u) curves for Hibond 77 from the pull-out tests (M.S.M. Laboratory)

3. Numerical simulation of a shear bond pull-out test

3.1 General

In this section, a finite element simulation of the pull-out test is presented in view to help us to understand better the shear bond mechanism between the steel sheeting and the concrete. The aim is to create a model, which -since we have proved its validation after a comparaison of its results with the experimental ones- can be used in the future, not only for examining the behaviour of the composite action (especially the shear bond mechanism) between the concrete and an existing at the

market steel sheeting in a composite slab, but also for optimizing an existing sheeting (by changing its geometry, its thickness or a parameter of its embossments, such as their geometry, position, height)) or for creating a new one; so, since the model is reliable and accurate, it won't be necessary to fabricate a new steel sheeting (each time we change a parameter) and to submit it to a pull-out test for examining its behaviour (gain of money and time).

A non-linear 3D finite element program, using large strains, developped at the M.S.M. Departement, has been the appropriate tool with which this objective was achieved. In this 3D analysis, the contact between concrete and steel is assumed without friction ($\phi = 0$) (or with a very small Coulomb's friction coefficient ($\phi = 0.1$) for numerical reasons); so, there is only one type of shear debonding between the cold-formed steel sheeting and the concrete, i.e. the mechanical resistance due to the embossments. In this way, one can insist more on the important role of the embossments which consist one of the most important factors determining the behaviour of a composite slab. For our numerical simulation, we used a profiled sheeting of type Hibond 77 (with thickness 0.88mm).

3.2 Discretization

Of course, the symmetry of the two profiled sheetings used in the test has been taken into account for the finite element simulation. As we want to treat the case of an infinite number of embossments, only a small part of the profiled steel sheeeting (that is to say a part of the sheet with one embossment) has been discretized.

3.2.1 General assumptions

In first approximation, the following assumptions were made: *(i)* there is no friction ($\phi = 0$) at the contact between the concrete and the steel sheeting and *(ii)* only yhe initial normal pressure (p) (resulting from the real weight of the concrete over the embossment) is acting on the embossment (the shear stresses τ_R and τ_S are neglected). With tese assumptions, there is a big difference between the numerical and the experimental results. That's why, for the next approximations, we modified and improved (since they are closer to the real conditions of the test) the above assumptions, as following: *(i)* a very small value of the Coulomb's friction coefficient is accepted ($\phi = 0.1$); this value is small enough, so that it is always only the machanical resistance due to the embossments which is the predominant type of the shear debonding but also, big enough (no zero), so that it permits the second condition to exist: *(ii)* take into account not only the initial pressure (p) (this time, calculated from the lateral force used in the pull-out test, which is expressed in terms of equivalent concrete weight; expressing the normal pressure in this manner provides a physical representation of the lateral forces involved and is independent of specimen width or length), but also the initial shear stresses (τ_R and τ_S), which is quite important, because of the angle of the embossments.

3.2.2 Concrete discretization

The concrete represents the foundation of the problem. It is assumed rigid and is piloted only on displacements. The whole foundation is completely fixed, except of the directio in which the equivalent lateral force is imposed on the pilot node. For the discretization of the concrete, a type of 3D triangular segment is used.

3.2.3 Concrete-steel interface discretization

The contact surface (the interface between the concrete and the steel sheeting) is discretized by a type of 3D mechanical contact element (with 4 or 8 nodes), connected with the upper face of the sheeting. For the contact, we used a constitutive law for unilateral thermo-mechanical contact (a coupled Coulomb 3D law) (adequate for a thermo-mechanical analysis of problems involving unilateral contact between two bodies; Coulomb dry friction is used; the contact condition is enforced via a penalty method or augmented Lagrangian method).

3.2.4 Steel sheeting discretization

For the steel sheeting, the following three discretizations were tried :
(1) the first discretization consists of 88 volume elements working on large strains (bricks with 20 nodes); for this case, 88 contact elements (with 8 nodes) and 528 triangular segments were used;
(2) the second discretization consists of 88 solid 3D mixed elements working on large elastoplastic deformations (with 8 nodes); for this case, 88 contact elements (with 4 nodes) and 176 triangular segments were used.

For these two discretizations, the same mesh was used (only the type of finite element for the steel sheeting discratization and the number of nodes were different). In spite of the advantages of the mixed elements of the second case (for our problem, they can give almost the same results as the 3D shell elements [2],which consists a more logical approach for a sheeting of small thickness), they are much more rigid from the brick elements of the first case, when, of course, the same mesh is used). That's the reason, we tried to refine the mesh of the second case (by divising each element to 4!) and we set about the third case:

(3) so, the third discretization consists of 4x88=352 solid 3D mixed elements working on large elastoplastic deformations (with 8 nodes); for this case, 352 contact elements (with 4 nodes) and 704 triangular segments were used.

In order that the procedure of the loading of the simulation was closer to the one of the pull-out test, we imposed a uniform displacement in the z direction to all the nodes of the sheeting along the side z=const.

For the steel sheeting discretization, the following laws were tried:
(i) an elastic constitutive law for solid elements at constant temperature (adequate for a mechanical analysis of elastic isotropic solid undergoing large strains) and
(ii) an elastoplastic constitutive law for solid elements at constant temperature (adequate for a mechanical analysis of elastoplastic isotropic element undergone large deformations; mixed or isotropic hardening is assumed, when the volume elements (bricks with 20 nodes) or the solid 3D mixed elements (with 8 nodes) are used respectively.

3.2.5 Results

In Fig. 4, the curves (R-u) (with R the reaction to the movement caused by the imposed displacements) are presented; as this figure shows, we tried each of the cases of the steel sheeting discretization for both elastic and elastoplastic laws.

4. Conclusions

Since actually the last case of the numerical simulation (with the third try of the steel sheeting discretization and an elastoplastic law) is not yet completed, general conclusions on the advantages and disadvantages of the different discretizations can not be formulated.

Shear-slip (R-u) curves for Hibond 77 (numerical simulations)
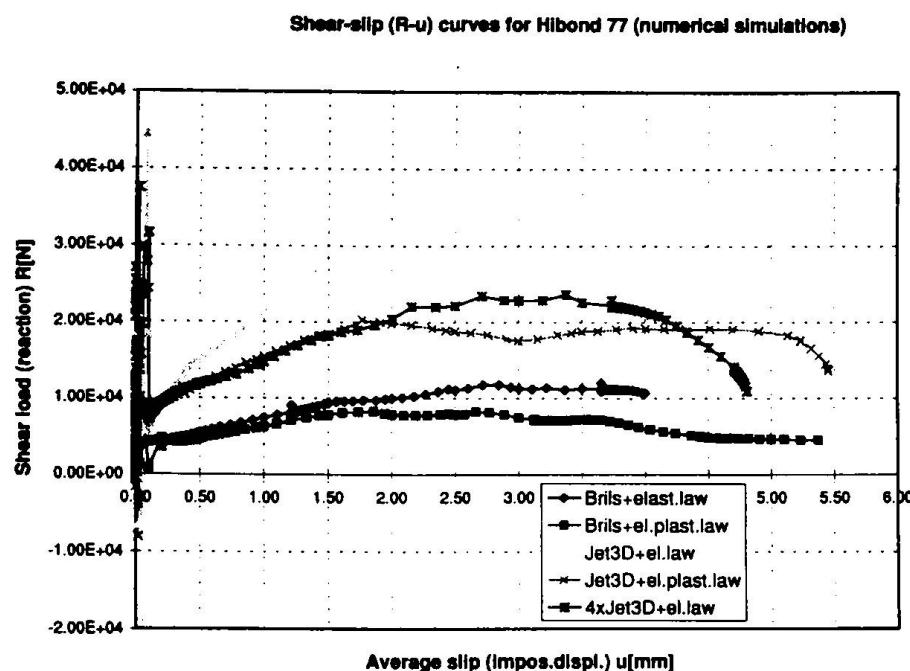
Fig. 4 Shear-slip (R-u) curves for Hibond 77 from the numerical simulation of the pull-out test.

References

[1] Daniels Byron J. , "Shear bond pull-out tests for cold-formed-steel composite slabs", Rapport d'essais, Ecole Polytechnique Fédérale de Lausanne, ICOM 194, Avril 1988.

[2] Kaiping Li , "Contribution to the finite element simulation of three-dimensional sheet metal forming", Thèse de doctorat, Université de Liège, Faculté des Sciences Appliquées, 1995.

Composite Slabs with and without End Anchorage under Static and Dynamic Loading

Helmut BODE
Professor Dr.-Ing.
Kaiserslautern Univ.
Kaiserslautern, Germany

Helmut Bode, born 1940 in Dresden,
received his Ph. Degree at Bochum Univ.
Since 1980 he is Professor of Civil
Engineering at the Steel Construction
Chair, Kaiserlautern Univ., Germany.

Frank MINAS
Research Assistant
Kaiserslautern Univ.
Kaiserslautern, Germany

Frank Minas, born 1963, received
his civil engineering degree in 1991
and since this time he investigates
the behaviour of composite slabs
at the Steel Construction Chair,
Kaiserslautern Univ., Germany.

Summary

This report deals with strength and behaviour of composite slabs with three typical, but different profiled steel sheet geometries used with and without end anchorage means (headed studs and bent rib anchors). A brief survey of slab design up to a modified global plastic analysis is given. Furthermore an improved partial shear connection method based on the results of small scale slip-block tests is introduced. In addition some results of slab tests with static and dynamic loadings are presented.

1. Introduction

This paper deals with the behaviour and design of composite slabs. Composite slabs consist of particular profiled metal deckings with concrete topping. They permit an easy and high speed construction of steel framed or even concrete buildings, whereby the steel sheet acts during erection among other things as safe working platform, permanent shuttering and horizontal bracing. After the concrete has hardened the profiled steel sheet is part or all of the tensile reinforcement. Their efficiency and advantages in combination with flexibility lead to an increasing use of composite slabs. Therefore the development of many different shapes all over the world is going on.

Numerous slab-, pull-out- and slip-block -tests with different types of composite slabs have also been carried out in the laboratory for structural engineering of Kaiserslautern University, Germany, in order to determine design values for their load carrying capacity and to investigate their behaviour. Till now in Germany in most cases Holorib-type metal decking is used. The new generation of these sheetings has embossments in the top flanges at least. But it shall be pointed out that trapezoidal composite slabs show also a similar ductile behaviour and high resistance in bending and longitudinal shear, if end anchorage means are applied. This end anchorage can be provided by throughwelded headed studs, which are anyhow necessary for the composite beam action. Objectives of our work and this paper are therefore

1. to enhance the resistance and behaviour of composite slabs with trapezoidals,

2. to improve the partial connection method which can be applied in designing composite slabs with ductile horizontal shear failure,

3. and to expand the range of application to cyclic loadings under fork lift trucks.

2. Ductile composite slabs

Basically three different types of metal decking are normally used on our construction sites:

- profiles with re-entrant shape (dovetail ribs, Holorib-type) without embossments, but together with end anchorage means, to create sufficient composite action,

- the Holorib-type sheeting with embossments (e.g. Cofrastra 40, Haircol, Super Holorib, SupeRip)

- and the trapezoidal profiles with embossments or idendations and with or without end anchorage means.

Trapezoidal shapes lead to a consumption of steel per m² flooring smaller than re-entrant profiles. However the vertical separation of the two composite partners is not efficiently prevented and therefore the longitudinal shear resistance is only about one tenth of the new generation of re-entrant profiles. The τ_u - values [1], [3] permit an easy comparison of the different metal decking types, see table 1.

profile geometry	failure mode without end anchorage	τ_u [kN/m²] (mean test value)
trapezoidal with embossments (Cofradal 60 t_N = 0.88 mm)	brittle	40
plain re-entrant (Holorib t_N = 0.88 mm)	brittle	120
re-entrant with embossments (Super Holorib t_N = 0.88 mm)	ductile	520

Table 1: Longitudinal shear resistance - Comparison for typical metal deckings

One outstanding advantage of re-entrant steel profiles is the fact that these composite slabs can attain a fire resistance of R90 without any supplementary reinforcement.

The load-deflection curves in figure 1 are test results, but they illustrate the typical behaviour of these three different types. Cross-sections, test set up and descriptions are in agreement with Eurocode 4 and quite similar for all curves: span length 3.0 m, shear span length L_S = L/4 = 750 mm, depth of composite slab h_t = 140 mm and nominal sheet thickness t_N = 0.88 mm.

Re-entrant profiles of the original generation (Holorib, without embossments) show a brittle failure mode. As soon as the pure shear bond is destroyed (increasing bending moment, cracking of concrete in tension, shear stresses on both sides of these cracks exceed the pure bond strength, end slip occurs) the load decreases suddenly and considerably. Due to clamping forces in the shear span length the re-entrant geometry makes somewhat higher loads possible.

Composite slabs with trapezoidal profiles (e.g. Cofradal 60) show also a brittle failure mode. But end anchorage means, in this case Cofradal 60 with throughwelded headed studs Ø 3/4" (19 mm), lead to a clear improvement of the slab behaviour up to failure, particulary with regard

to bending resistance and ductility. Almost no end slip occurs, and the sheet fails in load bearing at the headed studs at the panel ends.

The re-entrant shapes with embossments (new generation, e.g. Super Holorib) show however a very ductile behaviour, after first end slip has been recorded, together with high load carrying capacities. In this case significant slip occurs at the steel-concrete interface before the maximum load is reached (longitudinal shear failure). As an alternative, the ribs at the panel ends can be bent to provide another type of end anchorage and to prevent the wet concrete from flowing through the dovetail ribs.
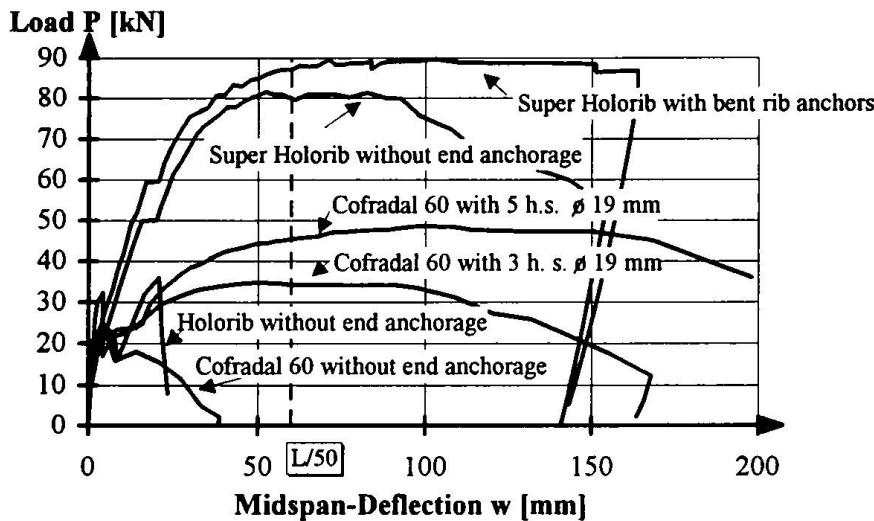
Figure 1:Load - deflection - curves for different profile shapes with and without end anchorage

A statistic evaluation of seven Cofradal 60 slab tests with throughwelded headed studs ∅ 3/4" leads to the characteristic shear strength $P_{pb.Rk}$ = 25.1 kN per stud. Eurocode 4 [1], 7.6.1.4 proposes for the load bearing capacity of headed studs corresponding to our test conditions the conservative value $P_{pb.Rk}$ = 19.6 kN. The evaluation of 23 earlier pull-out tests without concrete yields a load bearing capacity of such headed studs ∅ 3/4" being about 15.7 kN. The strengthening effect of the surrounding concrete results in about twice the value: from five pull-out tests with concrete a characteristic value of 31.3 kN per stud can be deduced.

A good approximation for the strength of one bent rib anchor is the area of the anchored rib times the yield strength of the steel sheet. For the Holorib 51/0.88 shape this leads to $P_{pb.Rk} = A_{Rib} \cdot f_{yp}$ = (3.6 + 2 · 5.1) · 0.88 · 32.0 = 38.9 kN.

3. Design methods for horizontal shear

Eurocode 4 offers two different design methods to check the horizontal shear strength of composite slabs.

The m+k - method - slightly modified from the original North Amercian version - is the standard method for the longitudinal shear verification.

The partial connection method (τ_u - method) with incomplete interaction and considerable relative displacements at the steel concrete interface is in accordance with the well known partial connection design for composite beams with flexible connectors. Therefore it can be used to design composite slabs with enough ductility even in case of horizontal shear failure. The same mechanical model is being used for the test evaluation and for design purposes (fig. 2a, b). This
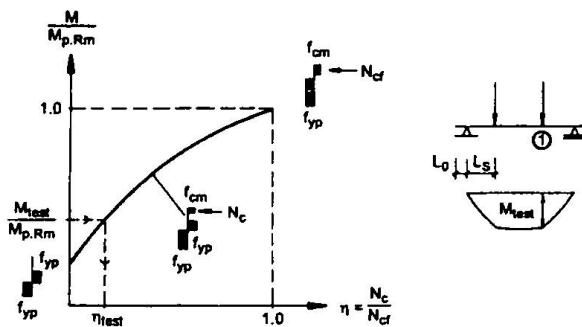
Figure 2a:Determination of the degree of shear
connection from slab test
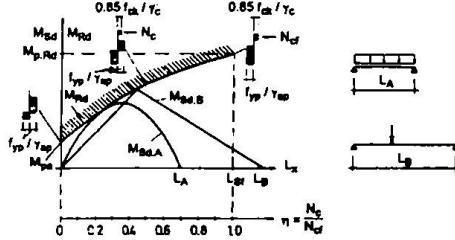
Fig. 2b:Design with partial interaction
diagram
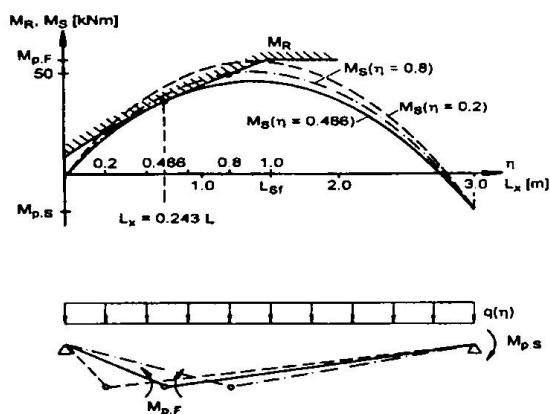
Fig. 2c:Design of continuous composite slabs

method leads to a very good agreement between theoretical solutions and test results. It is easy to take into account additional (fire) reinforcement and end anchorage measures. Even the determination of the ultimate loads of continuous composite slabs by means of a modified global plastic analysis is possible [5], [6]. Figure 2 shows this design method applied to a two span slab indcluding the critical cross section for η = 0.486 (degree of shear connection).

4. Improvement of the τ_u - method by means of slip-block tests

The evaluation of standard tests according to EC 4, annex E, results in the determination of τ_u as shown in figure 2:

$$\tau_u = \eta_{Test} * N_{cf} /(b * (L_S + L_0)) \qquad (1)$$

This shear strength τ_u consists mainly of the overriding resistance, but also of friction over supports and clamping forces, if there are any. Line 1 in fig. 3 indicates the overestimation of

Figure 3:Relationship between τ_u and the L_S/h_t ratio

longitudinal shear resistance for small L_S/h_t values. The filled round marks in fig. 3 indicate the τ_u - values of 13 full scale slab tests over the ratio shear span to depth (L_S/h_t). The tests with Super Holorib sheets were carried out and evaluated as shown in fig. 2 according to EC 4. Line 1 is a linear approximation throughout these 13 values. Results of the so called slip-block tests [8], [13] can be used to improve this method. Fig. 4 illustrates the test arrangement with a little composite

Figure 4:Test set up and test results of slip-block tests

slab specimen (e.g. length 300 mm, width 300 mm, high 200 mm) under vertical (V) and horizontal (H) loading. By means of this small scale test the contributions of friction (friction coefficient μ) and mechanical interlock (H_{mech}) can be separated. Fig. 4 contains test set up and test results of such slip-block tests carried out at Kaiserslautern University, and this with the same metal decking as used in the full scale slab tests. A linear regression analysis yields the corresponding friction coefficient. The remaining longitudinal shear resistance (after the contribution due to friction has been substracted) $\tau_u{}'$ results in line 2 in fig. 3. The square marks indicate the evaluation according to eq. 2. The influence of the shear span length is obviously clearly reduced, if friction over the supports is taken into account.

$$\tau_u{}' = \eta_{Test} * N_{cf} - \mu * V_{Test}/(b * (L_S + L_0)) \qquad (2)$$

5. Behaviour of composite slabs under cyclic loading

Load-deflection and load-slip curves of two identical slabs (Super Holorib 51/0.88) with preloading of 5000 cycles in the static test and with 2 Million load cycles in the dynamic test are compared in figure 5. In this case the maximum load itself, the midspan deflection at this load and the corresponding end slip are obviously independent of the number of load cycles. The major part (2/3) of midspan deflection increases along with concrete cracking and end slip during the first 5.000 cycles. The behaviour of this type of composite slab even under cyclic loading (from fork lift trucks) is very good, and no fatigue damage occurs as long as the stresses in the profile sheet are clearly lower than the yield strength. For the considered test the stress range $\Delta\sigma$ was 120 N/mm², and the top stress 75% of the yield strength. Tests with concentrated point loads are not described in EC 4. At the moment a research program with composite slab tests under static and dynamic loading (up to wheel loads of 7to forklift trucks) is carried out at Kaiserslautern University. As it can be seen from fig. 5, there is no difference between the static and dynamic tests regarding the maximum load. For fatigue design purposes it is proposed to assume rigid connection with full interaction
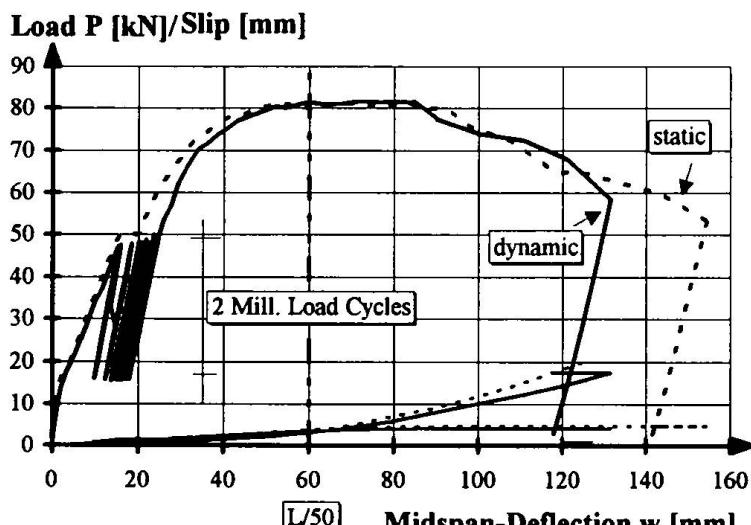

Figure 5:Load/ slip - deflection curves of static and dynamic slab tests

between concrete and profiled steel sheeting, in order to evaluate the stress range $\Delta\sigma$ in the steel part.

Now we are carrying out coupon tests with varying stress ranges $\Delta\sigma$ to derive values for further improved S-N-curves.

6. Conclusions

Composite slabs with ductile horizontal shear failure - such as re-entrant profiles with embossments or trapezoidal profiles with throughwelded headed studs as end anchorage means - show a very high load carrying capacity and good servicability properties under static and dynamic loading. This has been proved by means of composite slab tests. In addition a procedure has been outlined to improve the partial connection method by means of so called slip-block tests. This scientific work was financially supported by DFG (German Research Foundation). This support is gratefully acknowledged.

References

[1]   Eurocode 4: Design of Composite Steel and Concrete Structures - Part 1-1: General Rules and Rules for Buildings. ENV 1994-1-1:1992

[2]   National Application Document for Germany, DASt-Richtlinie 104

[3]   Bode, H.; Sauerborn, I.: Modern Design Concept for Composite Slabs with Ductile Behaviour. Engineering Foundation Conference on Composite Construction II, Potosi, USA. June 1992.

[4]   Crisinel, M.; O' Leary, D.: Composite Floor Slab Design and Construction. IABSE, Stuctural Engineering International Vol. 6, No. 1, 1996.

[5]   Bode, H.; Minas, F.; Sauerborn, I.: Partial Connection Design of Composite Slabs. IABSE, Stuctural Engineering International Vol. 6, No. 1, 1996.

[6]   Sauerborn, I.: Zur Grenztragfähigkeit von durchlaufenden Verbunddecken. Ph.D Thesis Kaiserslautern University, 1995.

[7]   Stark, J.W.B.; Brekelmans, J.W.P.M.: Plastic Design of Continuous Composite Slabs. IABSE, Stuctural Engineering International Vol. 6, No. 1, 1996.

[8]   Patrick, M.: The Slip Block Test - Experience with Some Oversea Profiles (Part A). Melbourne, Australia, June 1990.

[9]   Porter, L.: Two-Way Analysis of Steel-Deck Floor Slabs. Ninth International Specialty Conference on Cold-Formed Steel Structures St. Louis, Missouri, USA, 1988.

[10]   Crisinel, M.; Fidler, M.J.; Daniels, B.: Flexural Tests on Composite Floors with Profiled Steel Sheeting. École Polytechnique Féderal de Lausanne, March 1986.

[11]   Veljkovic, M.: Behaviour and Resistance of Composite Slabs. Experiments and FEM-Analysis. Ph.D Thesis, Lulea University, 1996.

Test and Analyses of a Bridge Continuous Composite Beam

Jean-Marie ARIBERT
Prof. des Universités
INSA
Rennes, France

Joël RAOUL
Ing. Ponts et Chaussées
SETRA
Paris, France

Olivier TERPEREAU
Assistant
INSA
Rennes, France

Summary

This paper deals with a test of a two-span continuous composite girder comprising sudden changes of cross-sections and mixed cross-sections (class 1 at mid-span and class 4 on internal support). Mainly the behaviour at serviceability limit state and ultimate limit state is presented. Also comparisons are made with different types of global analyses and with numerical simulation using a sophisticated software.

1. Introduction

In the frame of new concepts developed in Europe, particularly during the drafting of Eurocode 4 - Part 2 for composite bridges [1], some discrepancies with the French regulation [2] have appeared leading SETRA to order a two-span continuous composite beam test to INSA in Rennes. The loading procedure of this test has included several phases related to :
- the behaviour at serviceability limit state (non accumulation of deformations due to variable loads, cracking monitoring on the intermediate support) ;
- the resistance at ultimate limit state (maximum loads and possible redistribution of bending moments).

In parallel with this experimental approach, a specialized software has been developed on the basis of the finite element method specially adapted to the verification of composite bridge beams. This software is only used here for the simulation of the present test ; but in the future, it will be applied to the calibration of the various methods of analysis proposed in [1] covering a wider range of span lengths, different ratios between consecutive spans...

2. Test presentation

As shown in fig. 1, the tested composite beam comprises two continuous spans of 7.5 m and is subject to two independent concentrated loads P and Q each located at mid-span. This beam is class 1 at mid-span and class 4 on support A2 (due to the class 4 web). The bottom flange has a variable thickness (10 mm at mid-span, 15 mm on support A2) in order to simulate a composite bridge beam where the maximum resistance bending moments are reached almost simultaneously in sagging and hogging zones at ultimate limit state. Between the two loads, the web is heavily transversely stiffened to avoid a premature shear buckling.

The mechanical properties of the structural steel, reinforcement and concrete have been measured on several specimens leading to the characteristic values given in table 1.

	$f_y(MP_a)$	$f_u(MP_a)$		$f_{cm}(MP_a)$	$f_{ck}(MP_a)$
Web	480	570	Concrete	31.3	27.5
10 mm flange	385	540			
15 mm flange	465	585			
Reinforcement	475	610			

Table 1 . Material properties

Using these properties together with partial safety factors equal to 1, the mechanical properties of the composite cross-sections are as follows :

$I_1 = 12.3 \times 10^8$ mm^4 , $M^+_{pl.Rd} = 1166$ kN m   in sagging moment regions ;

$I_2 = 7.4 \times 10^8$ mm^4 , $M^{-(eff)}_{el.Rd} = 935$ kN m   in hogging moment regions.

During the casting of the slab, the steel beam was propped all along its length. The type of concrete was selected to minimize the effect of shrinkage ; so, the free shrinkage measured on an independent specimen of slab was equal to about 1×10^{-4} after one month. Due to this shrinkage and to the permanent loads, the stresses in structural steel and concrete have been estimated at -3.3 MPa (lower flange under load P) and $+ 1.2$ MPa (concrete in tension over A2) respectively.
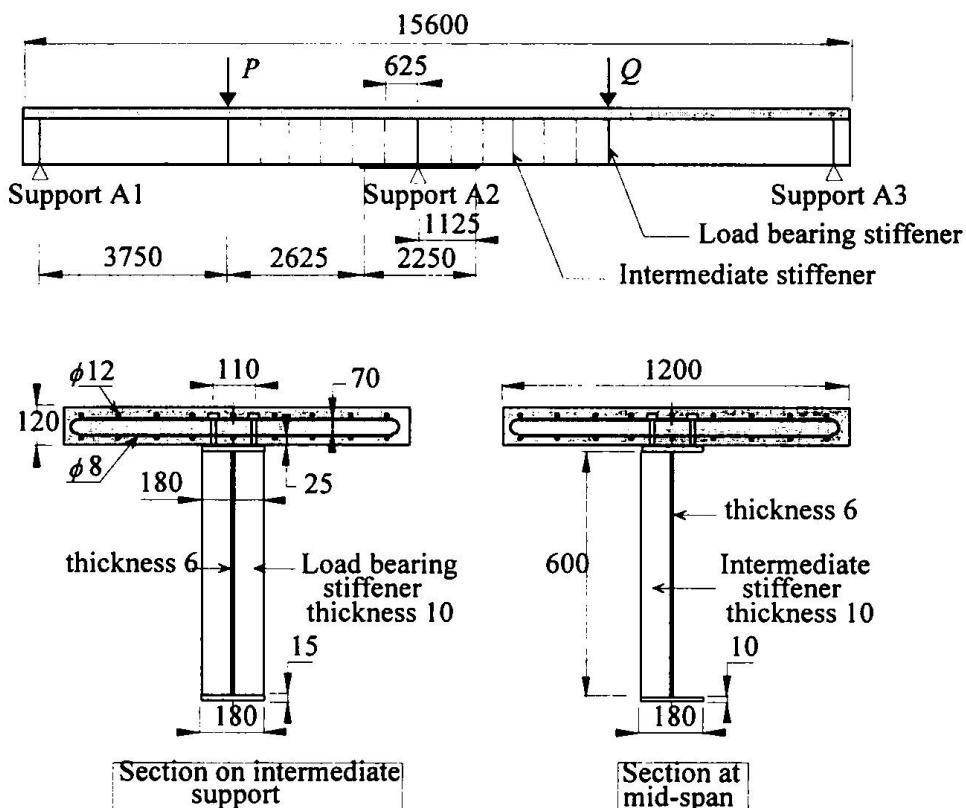

Fig. 1. Tested continuous composite beam

3. Test results and comparison with different types of analyses

The loading procedure comprises 123 phases. The main phases are summarized in table 2.

	Phase number	P(kN)	Q(kN)	Observation
Table 2. Loading procedure	8	100	100	• First cracks (0.1 mm) in the slab over intermediate support
	14	400	400	• Cracks 0.2 mm
Serviceability limit state	19 to 29	5 cycles 400-450-400	400	
	30 to 39	5 cycles 400-475-400	400	
	40	500	400	• First plastification in the lower flange under P (cracks ≤ 0.3 mm)
	41 to 48	5 cycles 400-550-400	400	
	61 to 66	5 cycles 400-550-400	400	
Ultimate limit state	93 to 101	P = Q from 0 to 550		
	101 to 113	550 to 810	550	• Shear buckles over the support
	122	890	550	• Beam failure

Figure 2 shows the variation of the beam deflection at the loading point P. Figure 3 shows the variations of the bending moments at mid-span (loading point P) and over the intermediate support (point A2). These moments have been derived from measurements of the bearing reactions at supports A1 and A3. They have also been checked against strain gauges measures on the steel flanges near support A2.
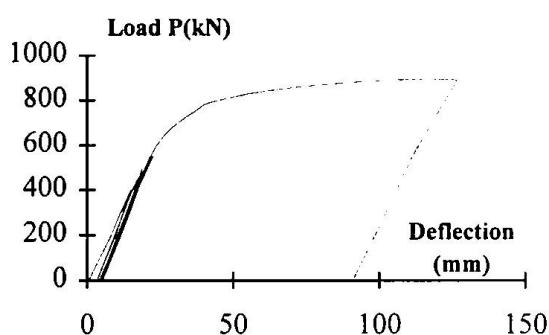
Fig.2 Load-deflection curve
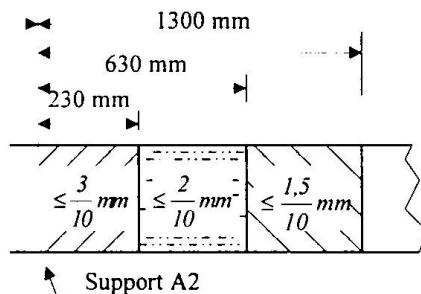
Fig.4 Distribution of crack widths

3.1. Serviceability limit state

(a) The first yielding appears during phase 40 for P = 500 kN and Q = 400 kN. A series of 5 cycles has been carried out around this loading (see table 2) and no cumulation of plastic deformation has been observed. But for phases 61 to 66 (P varying from 400 to 550), there is a more significant residual deflection (about 6% due essentially to the cracking of the slab obtained after the first cycle). This result tends to confirm the choice of a limitation of stresses of 1.0 f_y in the structural steel proposed in EC4-2 [1].

b) The crack widths have been carefully monitored up to phase 40 (S.L.S.). The reinforcement was designed according to EC4-1 [3] for a crack width of 0.3 mm. The distribution of the crack widths on each side of the intermediate support is shown in fig. 4.
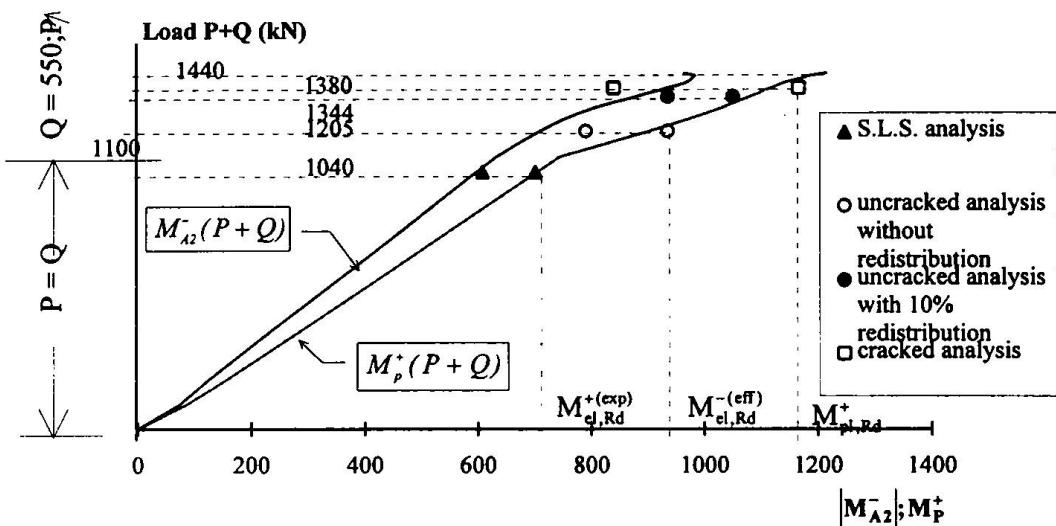
Fig.3 Variations of the bending moments at mid-span and over support A2

c) In fig. 3 related to the phases 93 to 122 (see table 2), the calculated bending moments at serviceability limit state have been plotted :

$$M_P^+ = M_{el.Rd}^{+(exp)} = 701 \text{ kNm (elastic bending resistance in the test condition)} ;$$

$$M_{A2}^- = -607 \text{ kNm,} \qquad \text{for :} \qquad P = Q = 520 \text{ kN.}$$

Elastic analysis has been used adopting a cracked zone over 15 % of the span length on each side of support A2. The plotted points fit perfectly with the experimental curves.

3.2. Ultimate limit state

(a) Three types of analyses according to EC4.2[1] have been compared :
- an « uncracked » analysis without redistribution giving :

$$P_u^{(1)} = 655 \text{ kN} \quad , \quad \text{with :} \quad M_{A2}^- = -935 \text{ kNm, } M_P^+ = 790 \text{ kNm}$$

- an « uncracked » analysis with a 10 % redistribution of the hogging bending moment at A2 leading to :

$$P_u^{(2)} = 794 \text{ kN} \quad , \quad \text{with :} M_{A2}^- = -935 \text{ kN m, } M_P^+ = 1050 \text{ kN m}$$

- a « cracked » analysis as in 3.1.(c) giving :

$$P_u^{(3)} = 830 \text{ kN} \quad , \quad \text{with :} \quad M_{A2}^- = -839 \text{ kNm} \quad , \quad M_P^+ = 1166 \text{ kNm}$$

All these calculated values of P_u are on the safe side in comparison with the experimental value $P_u^{(exp)} = 890$ kN. The high value of $P_u^{(exp)}$ is likely to have been allowed on account of redistribution of moments from mid-span to support A2. The points corresponding to the above analyses are plotted in fig. 3. In the present investigation, the « uncracked » analysis with a 10 % redistribution appears particularly appropriate whereas the « cracked » one tends to underestimate the bending moment on support A2.

(b) The shear plastic or buckling resistance has been verified in accordance with EC4.1[3] giving :

$$V_{Rd} = V_{ba.Rd} = 680 \text{ kN} \qquad \text{between A1 and P ;}$$

$$V_{Rd} = V_{pl.Rd} = 998 \text{ kN} \qquad \text{between P and A2 (aspect ratio of the web panels of about 1).}$$

That leads to a maximum ratio V_{Sd} / V_{Rd} of 0.57 close to 0.50. Consequently, the reduction of the calculated ultimate load P_u due to the vertical shear force is only 0.5 %.

(c) The connection was designed to resist the maximum possible shear flow at ultimate limit state (32 and 38 headed studs were welded between A1 and P and between P and A2 respectively, each having a shear resistance of about 100 kN).

(d) No lateral-torsional buckling has been observed during the test. But the calculation according to Annex B of EC4.1 (clause B.1.2) [3] would give $\bar{\lambda}_{LT}$ = 0.92 and a reduction factor χ_{LT} of about 0.6 , what seems to be a paradox. The very good behaviour of the tested beam can only be explained by the presence of the high density of vertical stiffeners welded to both flanges and to the web. By spreading and adding their stiffness to the flexural stiffness k_2 of the web (such a method is not in EC4.1), $\bar{\lambda}_{LT}$ becomes 0.37 < 0.40, what leads to χ_{LT} = 1.

4.   Numerical simulation

A numerical model based on the finite element method has been developed at INSA in Rennes using specialized beam elements (for steel and concrete), shear connector elements and buckling elements [4]. This model has been generalized for composite bridge girders by introducing other possibilities such as gradual or sudden changes of cross-sections, local buckling of web in class 4 (by means of the concept of effective depth), tension stiffening in slab after the stage of stabilized crack formation, and creep of concrete allowing to take into account the sequence of construction (this last aspect is not concerned in the paper) [5]. The effect of tension stiffening has been formulated in accordance with Annex L of EC4.2 [1] expressing the average tensile force N_s of the slab versus the average strain ε_{sm} as shown in fig. 5 (with factor β = 0.40).
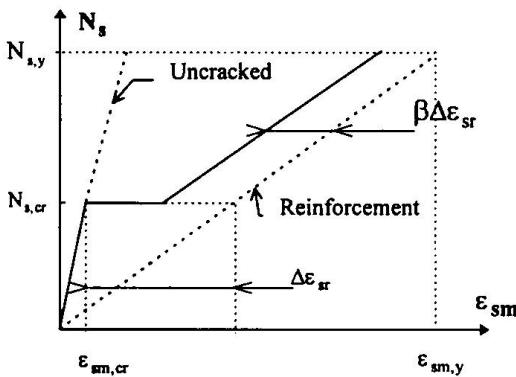
Fig.5 Tension stiffening curve
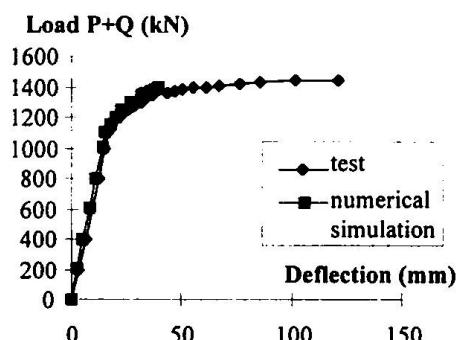
Fig.6 Comparison of the load-deflection curves

The composite beam tested above has been discretized using 186 finite beam elements and 68 shear connector elements. The simulated curve of the load versus the deflection (at the loading point P) is compared with the experimental one in fig. 6, showing a good agreement provided that a light additional deflection due to the vertical shear force in the web is taken into account for the elastic phase. Moreover, the simulated variations of the bending moments at mid-span and over support A2 are compared with the experimental ones (already given above) in fig. 7

and 8. But it is worth pointing out that the tension stiffening effect is only included in the simulation of fig. 7 and not in that of fig. 8. The better agreement in fig. 8 may appear a paradox though both simulations give the same ultimate load P_u. As explanation of such a paradox, it is possible to advance the gradual vanishing of tension stiffening during the test under the repeated cyclic loadings around the serviceability limit state. Also, some uncertainty of the real effective width of the slab in hogging moment zone may affect the results of the numerical simulation.
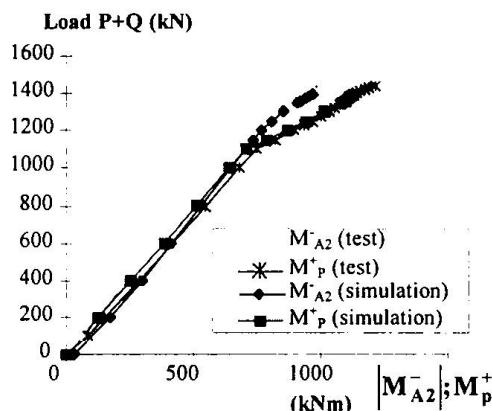

Fig. 7 Comparison of load-bending moments curves (with tension stiffening)
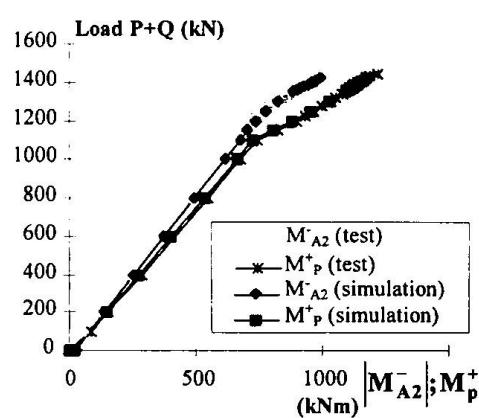
Fig. 8 Comparison of load-bending moments curves (without tension stiffening)

5.   Conclusion

The tested beam, representative of a composite bridge beam, confirms that the proposed methods to verify the serviceability limit state and the ultimate limit state in EC4-2 are safe and in rather good agreement with the experience. The software used for the numerical simulation gives results very close to the measured ones. It will be applied in the future to calibrate the analyses proposed in EC4-2 and to precisely define their scope.

References

1. Eurocode 4, « Design of composite steel and concrete structures », Part 2 :   « Bridges », ENV 1994-2, Third draft, CEN, Brussels, January 1997.
2. Ministères de l'Urbanisme, du Logement, des Transports et de l'Environnement, « Circulaire n° 81-63 relativement au règlement de calcul des ponts mixtes acier-béton », 28 juillet 1981.
3. «Eurocode 4, « Design of composite steel and concrete structures », Part 1.1, « General rules and rules for buildings », ENV 1994-1-1, CEN, Brussels, 1994.
4. Aribert, J.M. , Ragneau, E., et Xu, H., « Developpement d'un élément fini de poutre mixte acier-béton intégrant les phénomènes de glissement et de semi-continuité avec éventuellement voilement local », Construction Métallique, N° 2, 1993.
5. Aribert, J.M., « Chapitre 8 : Modélisation des ouvrages mixtes acier-béton avec leur connexion », Volume 1, Calcul des ouvrages généraux de construction (AFPC - Emploi des éléments finis en génie civil), Hermès, Paris, 1997.

Slenderness Limits for Thin-Walled Steel Concrete Filled Box Columns

Brian UY
Lecturer in Civil Engineering
University of Wollongong
Wollongong, NSW, Australia
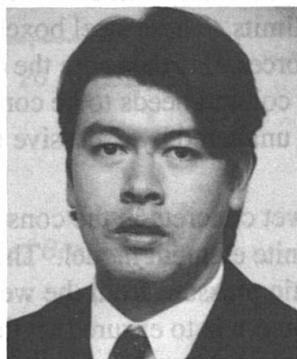
Brian Uy, born in 1970 received his Bachelors and Doctorate in Civil Engineering from the University of NSW. Since graduation he has worked on the design of multistorey buildings with Ove Arup and Partners, Sydney and he is currently lecturing in structural engineering. His main research interests include the application of composite construction in multistorey buildings.

Summary

This paper is concerned with slenderness limits of the thin steel plate used in the construction of concrete filled steel box columns. Requirements for limits on plate slenderness are outlined for construction, service and ultimate loads. Construction loading with regard to axial forces and hydrostatic pressure of wet concrete is considered and the time effects of concrete on the steel plate is studied for service loads. Finally inelastic and post-local buckling under ultimate loads is addressed and a set of experiments is used to calibrate a series of numerical models.

1. Introduction

The initial development of concrete filled steel columns saw the use of hot rolled steel sections for these members, (Bridge[1],Shakir-Khalil and Zegiche[2]). Hot rolled steel sections such as rectangular, square or circular sections used in the past were typically of plate thickness suitable to avoid local buckling when the columns were unfilled and hollow. The prevention of local buckling is important as it allows the columns to be designed to take full account of the steel strength. The relatively thick steel plate of hot rolled steel sections subsequently meant that for building construction, concrete filled steel columns were not widely used because of the exorbitant cost of using a steel section essentially as reinforcement. Their major use has been in highly seismic environments such as Japan where the thick steel sections prolonged local buckling and provided confinement to the concrete core. Furthermore the limitations of hot rolled steel section sizes manufactured as hollow steel columns has limited the geometric size of columns used which meant that for very tall buildings the sizes were unsuitable.

In Australia, a reassessment of concrete filled steel columns has been recently undertaken and consultants and contractors have developed techniques which allow these columns to be extremely competitive in terms of construction. Consulting Engineers, Ove Arup and Partners and Connell Wagner have utilised very thin walled fabricated steel box or tubular columns respectively to act as erection columns, (Watson and O'Brien[3] and Bridge and Webb[4]). These columns typically resist construction loads for several levels prior to the concrete being pumped inside. The use of these columns in Australia has been mainly in tall buildings where thin steel plate is utilised. This paper highlights the importance of each of the construction, service and ultimate loading stages for the choice of the slenderness limit of the steel plate used in these columns.

2. Construction Loading Stage

During construction, a concrete filled steel column is subjected to both axial force from the constructed levels in addition to the hydrostatic pressure from the wet concrete which is pumped inside. The economy of concrete filled steel box columns is influenced by the amount of steel and therefore the steel plate thickness used. Generally box columns are designed with very thin steel plate thus generating large slenderness limits. These steel boxes must be designed against yielding and buckling under the imposed axial forces. Furthermore the effects of wet concrete inducing hydrostatic pressure on the walls of the column needs to be considered so that the final constructed geometry of the columns is unaltered by excessive lateral deflections.

Uy and Das[5] studied the effects of the wet concrete in the construction stage of a concrete filled steel box column using a folded plate finite element model. The presence of the axial load from the constructed floors and the hydrostatic pressure from the wet concrete was incorporated in the analysis. During this stage the main concern is to ensure that the deformations caused by the imposed loads are minimised. The results of this analysis are summarised in the curves of Fig. 1 which shows the effects of the slenderness limit (b/t) and the number of levels being pumped, N_s on the maximum deflection of the column centreline.
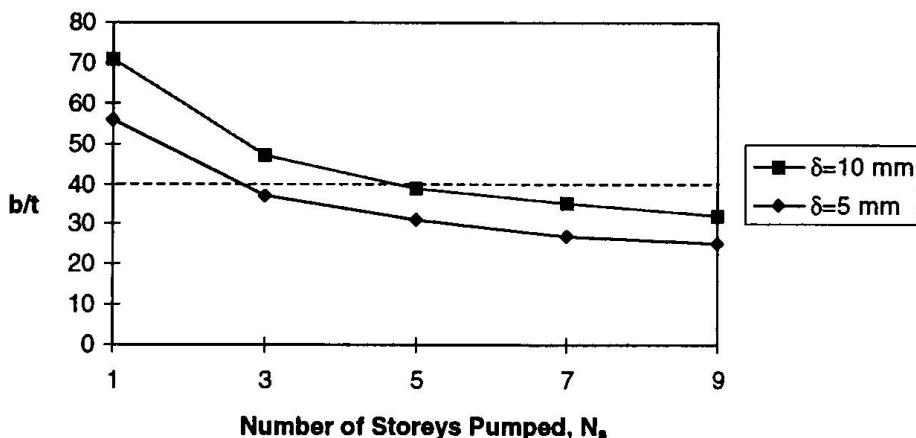

Fig. 1. Allowable Slenderness Limits for Wet Concrete Pumping (L=4,000 mm; b=1,000 mm)

A further study was carried out by Uy and Das[6] on the effects of intermediate bracing of concrete filled thin walled steel box columns. This study was undertaken to determine a strategy during construction to minimise lateral deflections without having to increase the steel plate thickness to excessive values which would render the method uneconomical. The study considered various bracing strategies while adopting slenderness limits which would be appropriate for ultimate strength and service loading. The results of a typical analysis with a column of 1,000 mm width and 4,000 mm height is shown in Fig. 2. The figure shows a deflection profile for a particular pumping strategy for a braced and unbraced column, where H is the height above the base of the column and δ is the lateral deflection of the steel plate. It is worth comparing the results of Fig. 1 with those presented in Fig. 2 for a column with a plate slenderness of 40. It is shown that in order to satisfy a maximum deflection of 5 mm, only two levels can be pumped without the presence of bracing. However the concrete can be pumped to five levels when three intermediate braces are used. This strategy is desirable for the construction of tall buildings as it greatly speeds the rate of construction and minimises the amount of steel plate necessary.
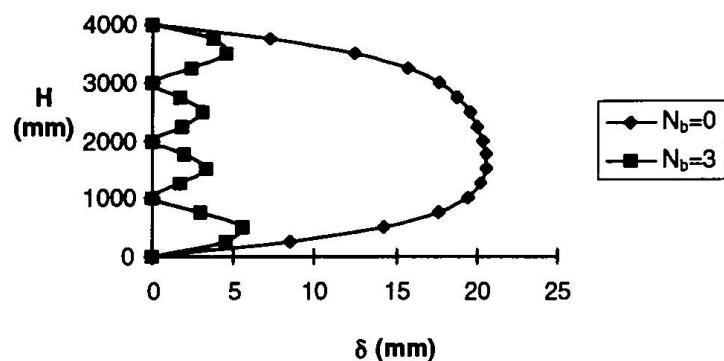
Fig. 2 Maximum Lateral Deflections of Box Column
(b/t=40; b=1000 mm, N_i=5)

3. Service Loading Stage

Uy and Das[7] have developed an age adjusted effective modulus method which allows for incremental loading and creep and shrinkage of the concrete for columns in a tall building. The effects of creep and shrinkage determined from experimental research by Terrey et. al[8] and Morino et. al[9] have been used in the determination of the stress redistribution and the total axial shortening of these columns. The analysis was carried out to consider a typical concrete filled steel column for a 60 storey building using a fairly large section.
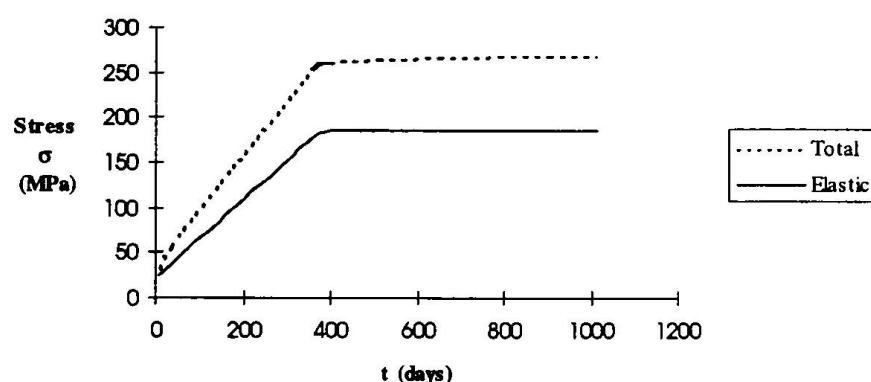
Fig. 3 Steel stress versus time

The results of the stresses and strains on a lower storey column were calculated as these would be the most heavily loaded columns in a building. The effects of creep and shrinkage of concrete in a concrete filled steel column will cause a redistribution of stress to the steel plate. This results in the steel stress increasing by 45 % from 180 MPa to 260 MPa as illustrated in Fig. 3. The effects of creep and shrinkage of the concrete on the slenderness limits are therefore significant and this illustrates that the onset of local buckling may occur prior to ultimate loads being reached.

4. Ultimate Loading Stage

Whilst it has been shown that the construction and service loading stages are very important and have an effect on the choice of the slenderness limit, it is the ultimate loading stage which usually governs the plate slenderness limit of a column. An optimum design requires that the steel box is able to develop it's full yield stress. One of the major advantages in allowing such a column to develop it's full yield stress is to ensure that the full amount of steel is being utilised prior to buckling. In order to identify appropriate values of the slenderness limit, two studies have been undertaken. Box column experiments were used to determine the local and post-local buckling behaviour of the columns. Furthermore an inelastic finite strip local buckling analysis was carried out and calibrated with the experiments.

4.1 Box Column Experiments

As part of a series of ultimate strength experiments on concrete filled steel box columns, several columns were tested purely to determine the local and post-local buckling behaviour of the steel plate by applying load to the steel box only. Table 1 outlines the dimensions and properties of these experiments. These experiments were useful in the determination of the local buckling stress in addition to the extension of a post-local buckling model originally developed by Uy and Bradford[10] for profiled steel sheeting. Table 1 also illustrates the yield stress σ_y and residual stress σ_r determined from tensile coupon tests and strain gauge measurements. The maximum load achieved N_{us} was recorded and the load at which buckling first occurred N_{ol} is given. The maximum load given by gross yielding is calculated as N_y. From these results the ratio of the local buckling stress to yield stress is determined and the effective width of the steel plates is also calculated. These will be used in comparison with the numerical models in the next section. A typical failure of these specimens is illustrated in Fig. 4 for specimen NS5 after inelastic local buckling has occurred showing the local buckle at mid height.

Test No.	b (mm)	b/t	σ_y (MPa)	σ_r (MPa)	N_{us} (kN)	N_y (kN)	N_{ol} (kN)	σ_{ol} (MPa)	σ_{ol}/σ_y	b_e/b
NS5	180	60	300	55	517	659	450	205	0.68	0.78
NS11	240	80	300	57	563	875	500	171	0.57	0.64
HS5	120	40	300	45	450	443	430	291	0.97	1.02
HS11	150	50	300	47	488	551	465	253	0.84	0.89

*Table 1. Local Buckling Tests*
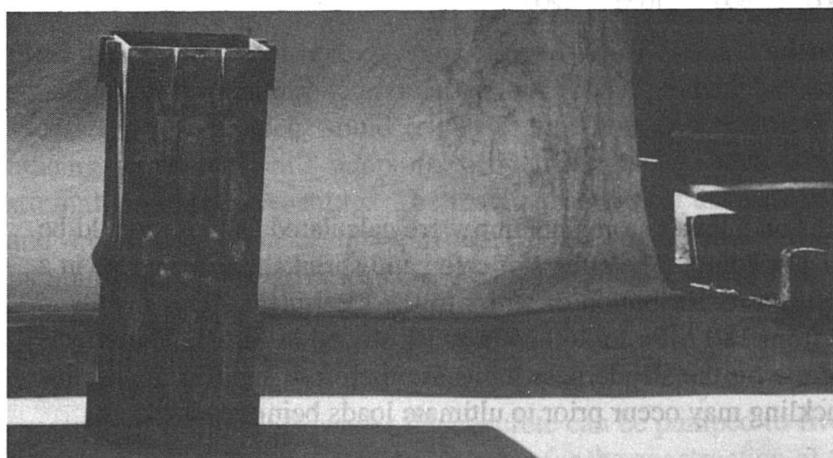
Fig. 4. Local Buckling Specimen NS5

4.2 Finite Strip Local Buckling Analysis

A finite strip method developed previously by Uy and Bradford[10] has been recently augmented by Uy[11] to consider the local buckling of welded steel box columns incorporating residual stresses. Results of this analysis are included in Fig. 5 which highlights the importance of the residual stresses in the elastic range. The box column experiments are also compared with the finite strip analysis in Fig. 5 and these suggest that the residual stresses of these columns are quite substantial. It should be noted that the local buckling stress is difficult to determine from tests and requires further investigation. The effective widths of the box columns are compared with the semi-empirical model of Uy and Bradford[10] and AS 4100[12] using a rational local buckling coefficient. The results illustrate the influence of residual stresses as the box column experiments allow less redistribution than profiled steel sheets. It is suggested that the AS4100[12] approach should be used as it is shown to be conservative.
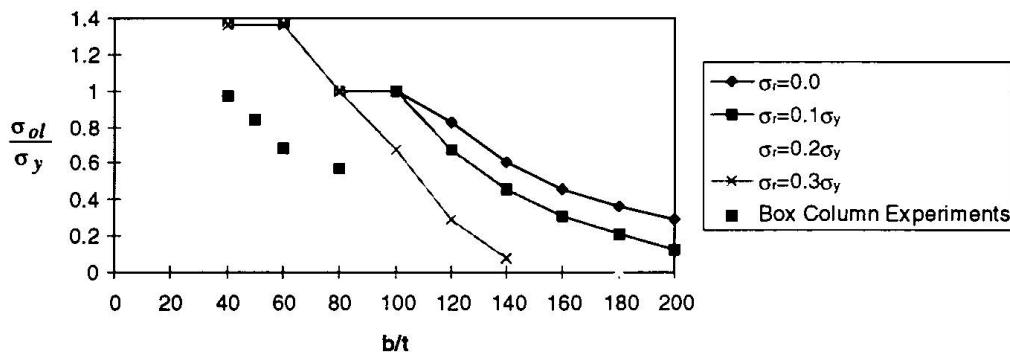

Fig. 5 Effect of Residual Stresses on Local Buckling Stress ($\sigma_y=300$ MPa; Pure Compression)
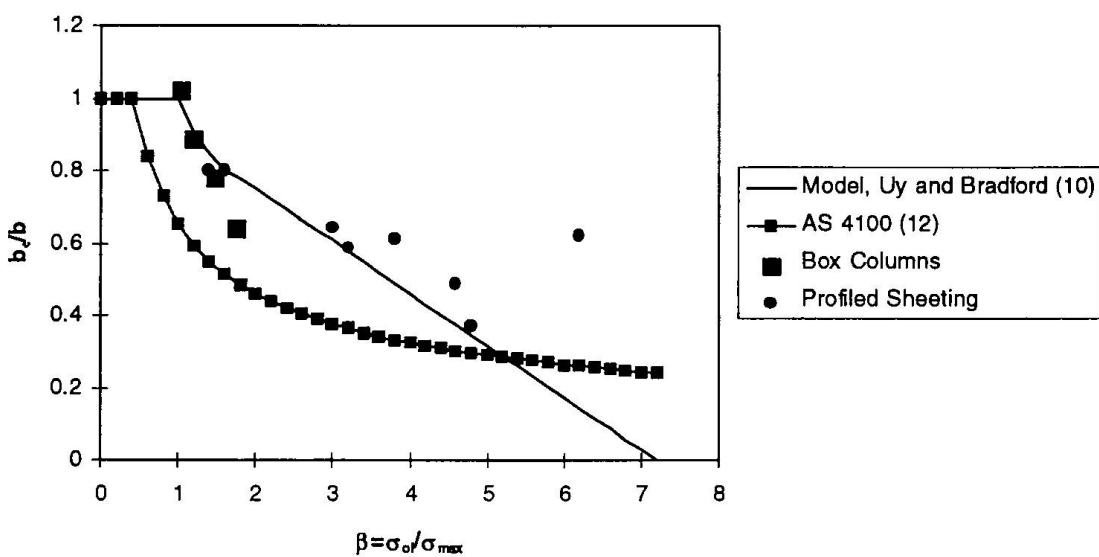

Fig. 6. Effective Width Model

5. Conclusions

This paper has presented research on the construction, service and ultimate load behaviour of the steel box in a concrete filled box column and has shown the importance of considering each of these loading stages for the steel plate slenderness selection. Further research is necessary and experimental work is currently being conducted into the construction, service and ultimate load behaviour of these members which will provide further data on the effects of the concrete on the steel plate.

6. Acknowledgements

7. References

1. Bridge, R.Q. Concrete filled steel tubular columns, Civ. Engg. Trans., Instit. of Engrs, Aust., 18 (2), 1976, pp.127-133.
2. Shakir-Khalil, H. and Zegiche, J. Experimental behaviour of concrete-filled rolled rectangular hollow -section columns, The Struct. Engr, 67 (19), 1989, pp. 346-353.
3. Watson KB and O'Brien LJ. Tubular composite columns and their development in Australia. The Institution of Engineers Australia, Struct. Engg. Conf., Adelaide, 1990, pp. 186-90.
4. Bridge, R.Q. and Webb, J. Thin walled circular concrete filled steel tubular columns, Comp. Constr. in Steel and Concrete II, Proc. of an Engg Found. Conf., 1992, pp. 634-649.
5. Uy, B., and Das, S. Wet concrete loading of thin-walled steel box columns during construction of a tall building, Submitted for publication.
6. Uy, B., and Das, S. Bracing of thin walled steel box columns during pumping of wet concrete in tall buildings, Submitted for publication.
7. Uy, B., and Das, S. Time effects in concrete filled steel box columns in tall buildings, The Struct. Des. of Tall Bldgs, 6, (1), 1997, pp. 1-22.
8. Terrey, P.J., Bradford, M.A., and Gilbert, R.I. Creep and shrinkage in concrete filled steel tubes, Tubular Structures VI, Proc. of the Sixth Int. Symp.on Tubular Structs, 1994, pp. 293-298.
9. Morino, S. Kawaguchi, J. and Cao, Z.S. Creep behavior of concrete-filled steel tubular members, Comp. Constr. in Steel and Concrete III, Proc. of an Engg Found. Conf., 1996 (In press).
10. Uy, B. and Bradford, M.A. Local buckling of thin steel plates in composite construction: Experimental and theoretical study. Structs and Bldgs,Inst. of Civ Engrs, 110, 1995, pp. 426-440
11. Uy, B. Local and post-local buckling of concrete filled mild and high strength steel welded box columns, Submitted for publication.
12. Standards Australia. AS 4100 Steel Structures, Australian Standard. Sydney, Australia, 1990.

Nonlinear Analysis of Composite Concrete-Filled Steel Tube Frames

Paul H. SCHILLER
Civil Engineer
Barr Engineering Co.
Minneapolis, MN, USA

Jerome F. HAJJAR
Assistant Professor
University of Minnesota
Minneapolis, MN, USA

Aleksandr MOLODAN
Graduate Research Assistant
University of Minnesota
Minneapolis, MN, USA

Summary

This paper outlines the formulation, calibration and verification of a three-dimensional, cyclic, distributed plasticity finite element model for composite frames composed of square or rectangular concrete-filled steel tube (CFT) beam-columns and steel wide-flange beams. The CFT model accounts for slip between the steel and concrete, and a brief study is presented which demonstrates that slip often has little effect on the global response of composite frames, although it may affect straining at beam-to-column connections.

1. Introduction

Research to date on CFTs has included tests on circular and rectangular columns, beams, beam-columns, and composite frames and trusses (Gourley et al. 1995), push-out tests to determine the bond strength at the steel-concrete interface, and connection studies to determine moment-rotation relationships and slip characteristics at connections (Hajjar et al. 1997a). However, relatively few computational models have been developed for analysis of composite frames composed of steel wide-flange girders framing into CFT beam-columns with fully-restrained or partially-restrained connections (termed "composite CFT frames"). This paper outlines the formulation of a finite element model for CFT beam-columns. This computational model is capable of accounting comprehensively for material nonlinear behavior at the stress-strain level, and for all significant geometrically nonlinear behavior. The resulting formulation is able to analyze complete three-dimensional composite CFT frames. This formulation has been verified against a large number of experimental results, and it may be used to assess the static and cyclic seismic behavior of individual CFT beam-columns, composite CFT subassemblages, or complete composite CFT frames. It is also suitable for conducting parametric studies to determine the significant factors which affect CFT behavior, including cross section geometry, constitutive behavior, slip characteristics, and end restraint, with the goal of developing improved design code recommendations.

2.   Finite Element Model

The current research utilizes a three-dimensional 18 degree-of-freedom (DOF) beam finite element developed by Hajjar et al. (1997a, b) to model CFT members. The formulation consists of a stiffness-based fiber element approach, in which the end cross-sections of each element are discretized into a grid of fibers, with the stress-strain behavior at each grid point monitored during the analysis. Through application of the material constitutive relationships, the spread of plasticity through the member end cross sections can be tracked. Linear shape functions are used to describe the change in member rigidity between the ends of the element. Traditional cubic Hermitian shape functions are used to describe the transverse deformation of the element between the end cross sections, and a quadratic shape function is used to describe the axial deformation (White 1985).

The current formulation models slip between the steel tube and concrete core of the CFT element along the element centroidal axis. The finite element model for slip follows the work of Amadio and Fragiacomo (1993), who developed a two-dimensional composite beam finite element which accounted for slip between an elastic steel girder and the concrete slab for monotonic loading. For the current CFT finite element formulation, three extra translational DOFs are added at each element end to permit the steel tube and concrete core to translate separately for a CFT which is arbitrarily oriented in space during a geometrically nonlinear analysis. The transverse displacements of the steel and concrete are constrained to be identical using penalty functions, thus allowing slip only along the longitudinal axis of the CFT, due either to flexural or axial loading. The separate axial DOFs are coupled through a layer of nonlinear slip springs along the material interface. Slip resistance is provided by friction and adhesion at this interface. The resulting computational model uses a bilinear load-slip relationship, with an initial stiffness (k_{slip}) up to the bond strength of the interface (f_{bond}), followed by a zero stiffness. This relation is representative of load-slip data seen in experimental studies of CFTs subjected to slip.

The current CFT finite element formulation extends the work of Amadio and Fragiacomo (1993) by including the significant geometrically and materially nonlinear effects which may be expected in CFT members subjected to cyclic loading. The formulation includes low and high-order geometrically nonlinear stiffness matrices to account for P-Δ and P-δ effects, and an updated Lagrangian incremental/iterative formulation to evaluate the stiffness matrices during the analysis. Lateral-torsional buckling, flexural-torsional buckling, and the bowing effect are not modeled. Additional details of the CFT finite element formulation can be found in Hajjar et al. (1997a).

3.   Nonlinear Material Models

Nonlinear material constitutive models are used to describe the stress-strain behavior of individual steel and concrete fibers at the member end cross sections. Both constitutive formulations are intended to model the full range of material stress-strain behavior commonly seen in CFT members, including capability to model repeated strain reversals under cyclic seismic loading.

The steel constitutive model used in the current formulation for structural steel wide-flange beams and for steel tubing is adapted from Shen et al. (1995). This bounding surface formulation

permits accurate prediction of the material tangent modulus during cyclic loading. The formulation was modified for modeling cold-formed steel tubing by including the variation in material properties within the tube cross section, and accounting for the gradual rounding of the stress-strain curve due to plastic straining during cold-working.

The concrete constitutive model is adapted from Ameur-Moussa and Buyukozturk (1990), supplemented by an elastic tensile branch prior to cracking. The compressive cyclic model is a combined plasticity-damage model with a vanished elastic zone. The scalar damage parameter accounts for micro-cracking in compression. The compressive model exhibits all important concrete behavior including stiffness degradation, hysteretic loading-unloading loops, and a descending post-failure branch. The tensile model includes tensile cracking and crack opening and closing upon repeated loading. The slope of the post-failure branch of the stress-strain curve was adjusted to match experimental moment-curvature-thrust results from monotonically loaded short CFT specimens (Tomii and Sakino 1979). This variation in the descending branch of the compressive stress-strain curve accounts for the added ductility of the concrete due to confinement of the concrete core by the rectangular steel tube. Calibration and verification of the steel and concrete constitutive models are described in Hajjar et al. (1997b).

4.   Calibration and Verification

Calibration of the slip model involved determining the appropriate values of k_{slip} and f_{bond} by utilizing the results from Dunberry et al. (1987) and Shakir-Khalil (1994) of CFT connection tests consisting of steel I-girders framing into CFTs with simple shear tabs. The initial stiffness k_{slip} = 10^4 MPa provided the best match to experimental results. This value results in computational solutions similar to analyses assuming perfect bond. However, modeling an accurate finite initial stiffness permits simulation of the gradual load transfer from the steel tube to the concrete core which takes place above and below the connection region. The calibration of bond strength resulted in a value of f_{bond} = 0.6 MPa. This value exceeds the design recommendations of both BS5400 (1979), which suggests a value of f_{bond} equal to 0.4 MPa, and AIJ (1980), which suggests a value of f_{bond} ranging from 0.1 MPa (for long term loading) to 0.15 MPa (for seismic loading). The difference in values may result from the use of connection tests in the current calibration, rather than push-out tests which were predominantly used for the development of these design codes. Connection tests were used for the current calibration rather than push-out tests because they are believed to represent more closely the conditions found in a CFT frame.

The current formulation has been verified against both monotonic and cyclic CFT experiments. The verification is presented in Hajjar et al. (1997a, b). Comparisons of two cyclic experiments with computational results are presented below together with the experiment schematics. Figure 1 shows a planar CFT specimen under constant axial load (P/P_0 = 0.2, where P_0 is the CFT axial strength) and cyclic shear loading (Sakino and Tomii 1981). Figure 2 shows a three-dimensional cruciform subassembly composed of steel wide-flange beams framing rigidly into a rectangular CFT column, with constant axial (P/P_0 = 0.15) and out-of-plane beam loading, and alternating antisymmetric in-plane beam loading to simulate seismic loads (Morino et al. 1993).

Tube: 100x100x4.21

f_y = 295 MPa

f_c = 24.0 MPa

L/D = 6.0

D/t = 24.0

··· Experiment (Sakino et al. 1981)   ─── CFT Fiber Model
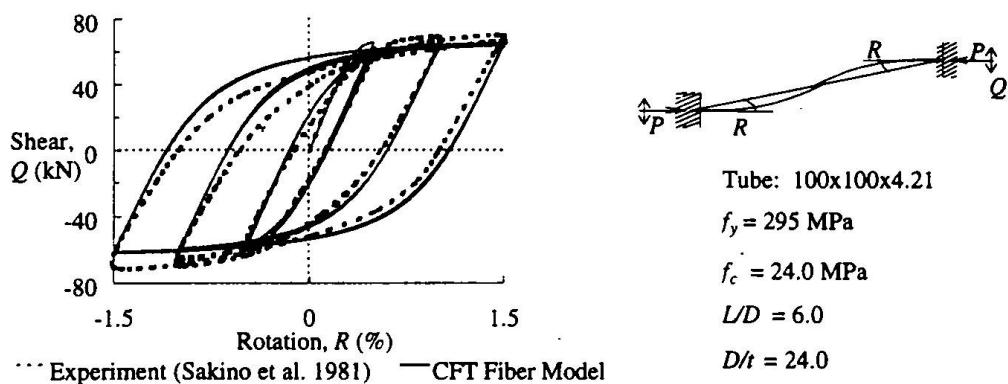
Figure 1: Comparison of Computational and Experimental Results (Sakino and Tomii 1981, Specimen CIVS3-2)

Tube: 125x125x5.74

f_y = 395 MPa L/D = 18.0

f_c = 20.0 MPa D/t = 22.0

··· Experiment (Morino et al. 1993)   ─── CFT Fiber Model
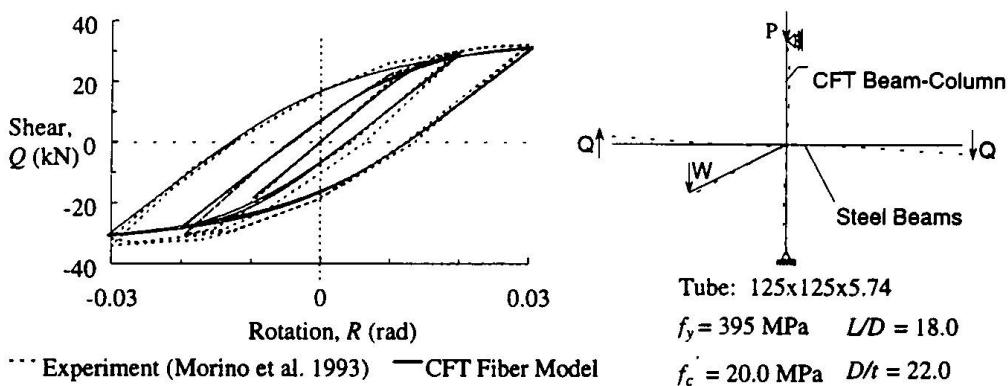
Figure 2: Comparison of Computational and Experimental Results (Morino et al. 1993, Specimen SCC-20)

5.   Effect of Slip on CFT Members and Composite Frames

Only limited studies have been conducted on the effect that slip has on the load-deformation behavior and ultimate strength of CFT members (e.g., Dunberry et al. 1987; Shakir-Khalil 1994). The AISC LRFD Specification (1993) limits the ultimate flexural capacity of CFTs to the plastic moment capacity of the steel section alone, partially due to the lack of data on slip. This limitation reduces the economy of CFTs as the primary lateral load resisting elements in unbraced frames. The formulation in this work may be used to provide supplemental data for determining the effect of slip on CFT behavior.

A preliminary study of the effect of slip on CFT flexural capacity and moment-curvature behavior was conducted for three CFT cross sections with different tube width-to-thickness ratios by varying both f_{bond} and k_{slip} from the calibrated parameters. Reducing k_{slip} by two orders of magnitude slightly reduced the rigidity of these members, but had no perceptible effect on the ultimate moment capacity. Reducing f_{bond} to 0.1 MPa [e.g., a value in the range of that

recommended by AIJ (1980)] reduced the computed moment capacity of the CFTs by 3% to 5%, suggesting that bond strength may have a small effect on the moment capacity of CFTs.

A second study was conducted to determine the effect of slip on frame behavior. Figure 3 shows a 4-story 4-bay frame subjected to factored gravity and wind loading. The loads are increased proportionally until the collapse of the frame is detected. Four cases were investigated to determine the effect of boundary conditions and slip parameters on the behavior of the frame. In Case I, the steel girder is assumed to engage the concrete directly through the connection, and no slip is permitted at the joints. In the other cases, the steel girder is assumed to engage only the tube, and load is transferred to the concrete through the slip interface. No perceptible difference in the global load-deformation response of the structure was observed between the four cases. An investigation of the interface stresses for Cases II, III and IV indicates that the values of both f_{bond} and k_{slip} affect whether bond strength is surpassed in a CFT frame. Bond loss is not detected for Cases II and III, although values close to 0.6 MPa are seen in Case II. However, Case III has interface stress values which are approximately 35% of the values for Case II, because for Case III the transfer of load at the connections occurs over a larger length of the CFT due to the lower stiffness. For Case IV, the bond strength is breached in several locations (first breach occurs at 19% of the design loading) resulting in localized slip in the connection regions that is approximately five times that seen in Case II (although the slip magnitudes remain small).
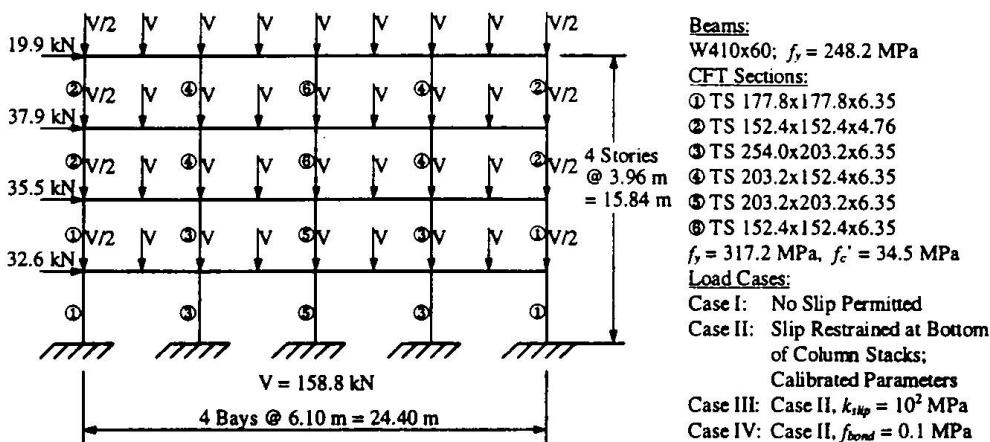

Figure 3: Composite CFT Frame Model

6.   Conclusions

The computational formulation presented in this paper is suitable for conducting parametric studies of individual CFT members and complete composite CFT frames. This formulation may also be used to determine the effect of slip stiffness and bond loss on rigidity, ultimate strength, ductility, and monotonic or cyclic behavior of composite CFT frames. A preliminary study demonstrates that the ultimate moment capacity of flexural specimens shows only slight change by lowering the bond strength. Variations in slip stiffness and bond strength are also seen to have virtually no effect on the global response of a CFT composite unbraced frame, although the slip parameters do have a small effect on the CFT behavior specifically in the connection region.

Acknowledgments

References

American Institute of Steel Construction, Inc. (AISC) (1993). "Load and Resistance Factor Design Specification for Structural Steel Buildings." Second Edition, AISC, Chicago, IL.

Ameur-Moussa, R. and Buyukozturk, O. (1990). "A Bounding Surface Model for Concrete." *Nuc. Engrg. Des.*, 121, 113-125.

Architectural Institute of Japan (1980). *AIJ Standard for Structural Calculation of Mixed Tubular Steel-Concrete Composite Structures.* AIJ, Tokyo, Japan.

BS 5400 (1979). *Steel, Concrete, and Composite Bridges: Part 5: Code of Practice for Design of Composite Bridges.* London, British Standards Institution.

Dunberry, E., LeBlanc, D., and Redwood, R. G. (1987). "Cross-Section Strength of Concrete-Filled HSS Columns at Simple Beam Connections." *Can. J. Civil Engrg.*, 14, 408-417.

Gourley, B. C., Hajjar, J. F., and Schiller, P. H. (1995). "A Synopsis of Studies of the Monotonic and Cyclic Behavior of Concrete-Filled Steel Tube Beam-Columns." Rep. ST-93-5.2, Dept. of Civil Engrg., U. of MN, Minneapolis, MN.

Hajjar, J. F., Schiller, P. H., and Molodan, A. (1997a). "A Distributed Plasticity Model for Concrete-Filled Steel Tube Beam-Columns with Interlayer Slip." *Engrg. Struc.*, sub. for publ.

Hajjar, J. F., Molodan, A., and Schiller, P. H. (1997b). "A Distributed Plasticity Model for Cyclic Analysis of CFT Beam-Columns and Composite Frames." *Engrg. Struc., Spec. Vol.*, at press.

Morino, S., Kawaguchi, J., Yasuzaki, C., and Kanazawa, S. (1993). "Behavior of Concrete-Filled Steel Tubular Three-Dimensional Subassemblages." *Comp. Const. in Stl. and Conc. II*, Easterling, W. S. and Roddis, W. M. K. (eds.), Engrg. Found., ASCE, NY, 726-741.

Sakino, K. and Tomii, M. (1981). "Hysteretic Behavior of Concrete Filled Square Steel Tubular Beam-Columns Failed in Flexure." *Trans., Japan Conc. Inst.*, 3, 439-446.

Shakir-Khalil, H. (1994). "Beam Connection to Concrete-Filled Tubes." *Tubular Structures VI*, Grundy, P., Holgate, A., and Wong, W. (eds.), A. A. Balkema, Rotterdam, 357-364.

Shen, C., Mamaghani, I. H. P., Mizuno, E., and Usami, T. (1995). "Cyclic Behavior of Structural Steels. II: Theory." *J. Eng. Mech.*, ASCE, 121(11), 1165-1172.

Tomii, M. and Sakino, K. (1979). "Elasto-Plastic Behavior of Concrete-Filled Square Steel Tubular Beam-Columns." *Trans., Arch. Inst. Japan*, 280, 111-120.

White, D. W. (1985). "Material and Geometric Nonlinear Analysis of Local Planar Behavior in Steel Frames Using Interactive Computer Graphics." M.S. th., Sch. of Civil and Envirn. Engrg., Cornell Univ., Ithaca, NY, August.

Experimental Verification of Bearing Capacity
of Composite Truss Girders

Zbigniew MARCINKOWSKI
Structural Engineer
Technical University
Wroclaw, Poland

Zbigniew Marcinkowski, born in 1937,
obtained his PhD from the Technical
University of Wroclaw in 1975. He
worked for six years as a manager
in a construction enterprise making
long-span pre-stressed plates. His main
research interest is connected with
industrial building engineering.

Piotr BERKOWSKI
Structural Engineer
Technical University
Wroclaw, Poland

Piotr Berkowski, born in 1957
received his PhD from the Technical
University of Wroclaw in 1986. He spent
two years with a research grant at the
University of Zaragoza, Spain. His present
research interests focus on structural
optimisation and structural design.

Summary

A frequently applied roof form covering industrial shops is a structure which consists of thin-walled reinforced concrete precast slabs laid on steel truss girders. The structural continuity is assured by means of reinforced concrete curbs cast-in-place on the truss top flanges. A statical analysis of such a structure considered as a composite one had been performed. This model represents quite well the real work of the structure. The calculation results have been positively veryfied by means of experimental research.

1. Introduction

A blocked, five bay production shop of a copper ore enrichment plant has its dimensions in plan 225.6 x 135.0 m. The cross-section of the production building is shown in Fig. 1, while the general view of the researched truss girders is presented in Fig. 4. The bays have their heights respectively 18, 25, 34, 25 and 18 m. Each bay is fitted out with two overhead cranes. The heaviest overhead crane has its bearing capacity of 160 T. The main load carrying structure consists of steel and reinforced concrete frames spaced every 6.0 m. The necessary rigidity in the plan of frames is provided by the middle bay, constructed in the form of reinforced concrete, monolithic bunkers for crumbled ore. Arrangement of longitudinal and transversal walls of these bunkers can be considered as a solidly reinforced concrete shaft.

Simply-supported steel truss girders of 30, 30, 15, 30 and 30 m span and laid on them prefabricated thin-walled reinforced concrete slabs, of 6 m span, are used as structural elements of the roof. These slabs have been manufactured in Poland for 45 years as typical elements of industrial shop roofs. Partial corrosion of top flanges of roof girders has been observed after 22 years of exploitation. The object should be still exploited for at least 30 years. There exists consequently a necessity to qualify the bearing capacity of roof girders.

Bearing capacity had been qualified by means of: 1) a standard calculation procedure as for flat lattice elements, taking into consideration reduction of top flange cross-section because of corrosion; 2) taking into consideration a composite model of a truss girder top flange. The calculated bearing capacity of truss girders is greater than the acting load.
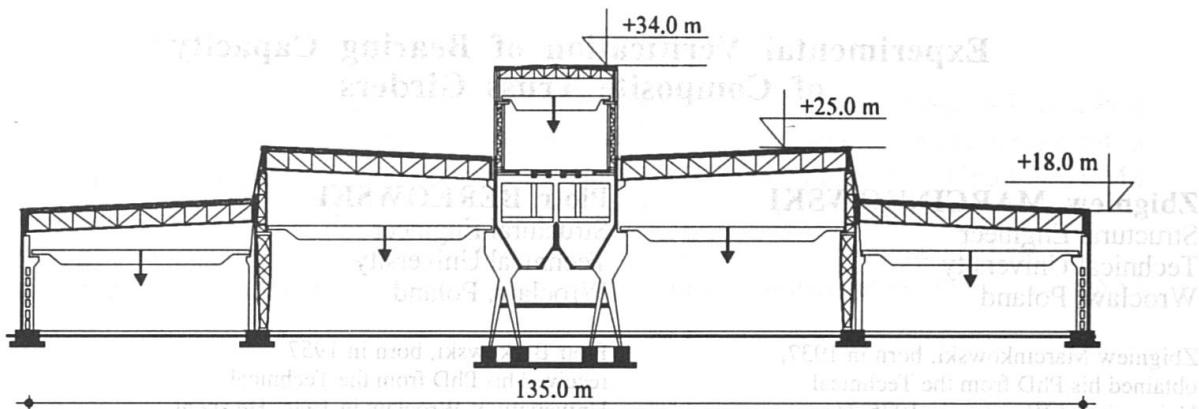
Fig. 1 Transversal section of the blocked five bay shop

Bearing capacity of the main structural elements of the roof decides the global safety of the object. Therefore it was recognized as advisable and necessary to get information about bearing capacity of these girders from another, independent source of information. To this aim the existing deflection of 72 girders was measured and that provided a sufficient number of tests for statistical elaboration of research results.
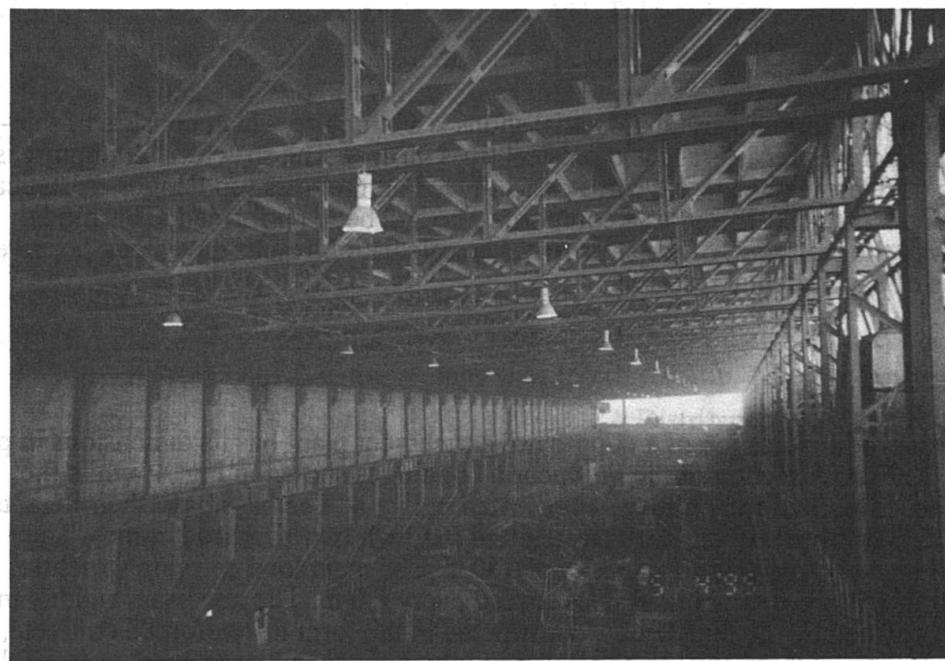
Fig. 2 General view of the researched roof truss girders

2.   Principles of co-operation between steel and concrete in composite structures

Slender and thickset bent beams and columns are the most often type of composite steel-concrete structures used in building engineering. The static model of a compressed top flange of examined roof girder can be considered as a compressed composite section as shown in Fig. 3. In conformity with the Polish Code PN-91/B-03302 which takes into account the requirements of Eurocode 4 within the domain of composite action of concrete and steel, namely that the connection of steel with concrete should be assured if tangential stress τ appears in the contact surface between these two materials. This condition is satisfied beacuse the reinforced concrete curb (3) is mechanically linked to the batten plates (2).
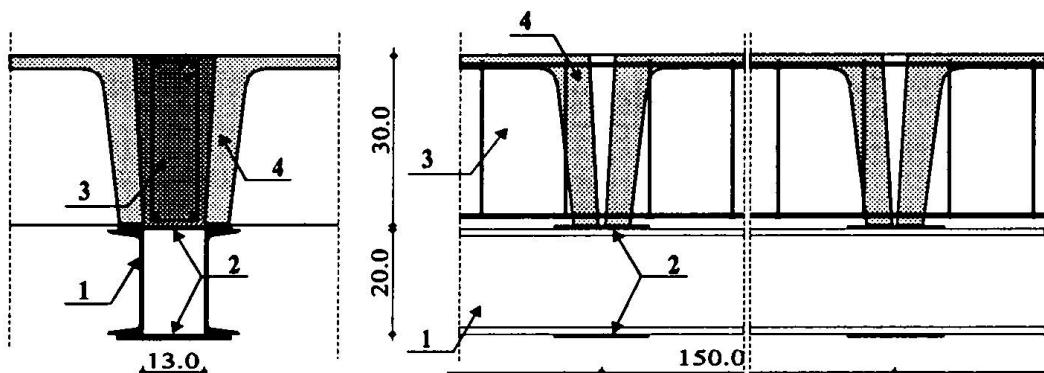
Fig. 3   Composite section of a truss girder top flange: (1) - steel top flange of a girder,
(2) - batten plates connecting branches of a girder flange, (3) - R/C curb,
(4) - precast thin-walled reinforced concrete slabs 30x150x587 cm

Connectors between steel and concrete are not necessary, if tangential stress τ in connection plane is less than 0.6 MPa. In our case tangential stress caused by:
- temperature difference,
- shearing forces and bending at intervals between nodes,
- concrete shrinkage

is $\tau < 0.8$ MPa. It signifies, that batten plates (2) - connectors between steel and concrete are not loaded. Bearing capacity N_{pl} of a composite section, according to PN-91/B-03302, is given by:

$$N_{pl} = F_s \cdot R_s + 0.85 \cdot F_b \cdot R_b + F_a \cdot R_a,$$

where: F_s, F_b, F_a - cross-section areas of steel, concrete and reinforcement; R_s, R_b, R_a - strength of steel, concrete and reinforcement. This equation was used while determining the state of stress and strain in the examined composite section, as part of a truss girder.

3.   Calculation scheme of truss girder

A statically determined truss, as in Fig. 4., was accepted as the scheme for calculation.
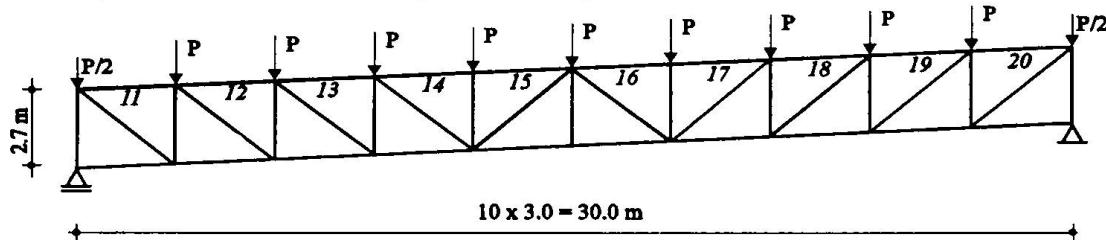
Fig. 4   Calculation scheme of truss girder

The force P is a dead load for which the girder's deflection line is calculated.
The girder works in two phases:
- in phase I the load has the value of $P_m = 32.09$ kN. This load works during assembling the roof elements and is carried only by steel girder;
- in phase II the load has the value of $P = 78.73$ kN. The composite steel-concrete section of truss girder top flange, as in Fig. 3, takes part in carrying the load from the level P_m to P.

Phases of truss girder work are illustrated in Fig. 5, that presents the relation between load and displacement: $P = P(f)$. A diagram presenting $P = P(\sigma)$ would be very similar. Introduction of an equivalent stiffness of truss girder would be useful for interpretation of information presented in Fig. 5. In phase I, that is to the load level corresponding to load P_m existing while assembling the structure, and the top girder works as a "pure" steel truss. The equivalent stiffness $(EJ)_1$ is proportional to tg α_1. During phase II, it is above the load level P_m existing while assembling, the girder works as a composite steel-concrete element. The equivalent stiffness
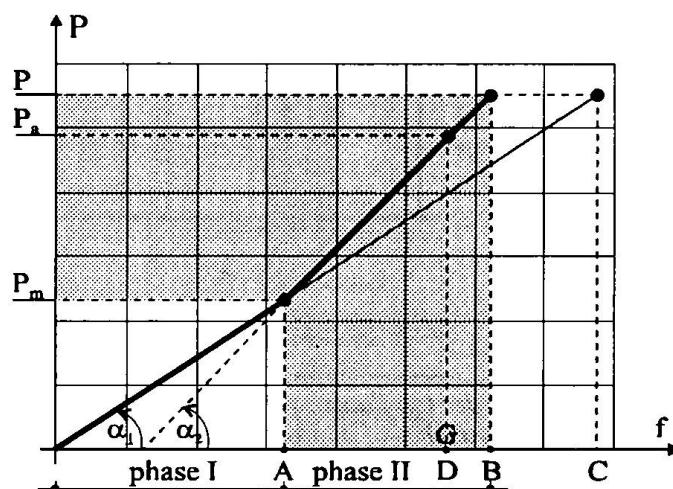
Fig. 5 Relation P = P(f) for phase I and II of a girder's work path. Notations: A, B, C, D - displacements of a middle point of a girder from: characteristic assembling load P_m, characteristic total load P - for a composite model, characteristic total load P - without accounting for concrete co-operation, characteristic real load P_a

$(EJ)_2$ of the composite section is proportional to tg α_2. It is worth stating that $(EJ)_2 > (EJ)_1$. In the examined problem $(EJ)_2 = 1.16 \cdot (EJ)_1$. It indicates that the girder equivalent stiffness after assembling increased about 16%.

To verify experimentally the presented calculation model, the deflection measurement of 72 truss girders were carried out. Deflection measurements were realized for real state of load P_a. The obtained mean deflection value of truss middle joint (point G in Fig. 5) precisely corresponds to the expected result delivered for a composite structure working in phase II.

4. Results of geodetic measurements of truss girders' deflections

The aim of geodetic measurements of vertical displacement of roof girders was an experimental verification of the supposition that examined roof girder works in two phases:
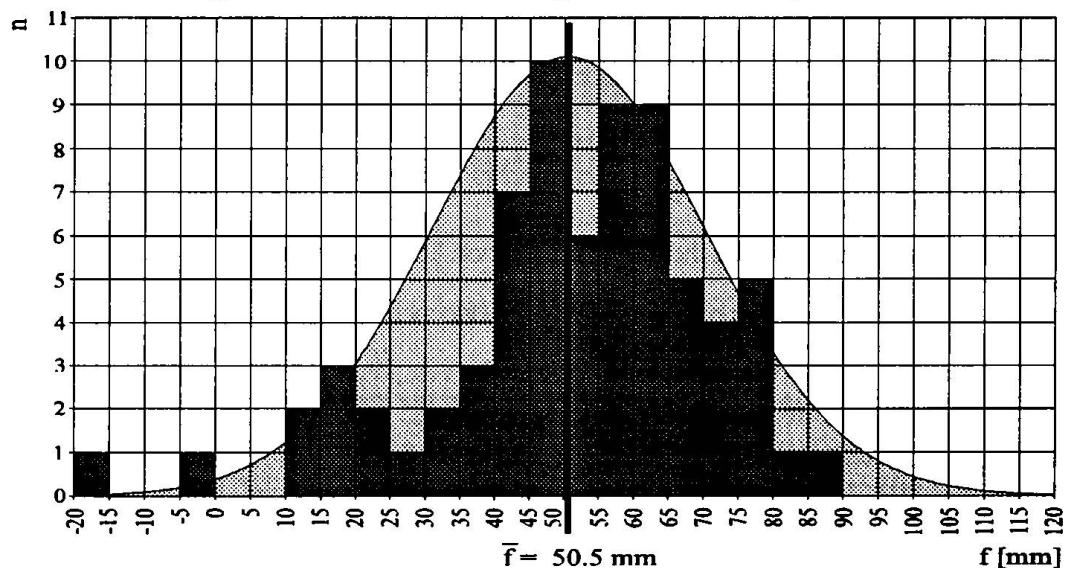

Fig. 6 Histogram and diagram of normal distribution of the geodetic measurement of roof girders' displacement

- phase I - the load level corresponding to load P_m existing while assembling - as a "pure" steel truss;
- phase II - above the load level P_m - as a steel-concrete composite structure.

Measurement of 72 truss girder deflection was carried out. The synthesis of measurement results is presented in Fig. 6 as a histogram.

A population of measurement results was divided into fractions of d = 5 mm width. Conclusive value of measured deflection is the arithmetic average of measurement results, because it is an unbiased estimator of expected value. Its value is $\bar{f}$ = 50.5 mm, as shown in Fig. 6. The results of measurements, approximated by a normal Gauss distribution, have a following statistical parameter: n = 72, $\bar{f}$ = 50.5 mm, v = 39%, Δ = 19.75 mm. Deviation of geodetic measurement from the average value of $\bar{f}$ defines a girder geometric production imperfection. This interesting problem was not developed in this work because of the lack of space.

5. Comparison of stress and deflection calculation results with experimental measurements

In Tab. 1 stresses expected from calculation to appear in the top flange of roof girder are presented for two models of girder construction:
- traditional model - structure works as a separate steel truss;
- real model - a top flange works as a composite steel-concrete section.

Tab. 1 Specification of force and stress in a composite steel-concrete top flange of a roof girder

Member number - Fig. 3	Member area F_s	Assembling load P_m		Total load P		Equivalent area of composite section	Load in phase II (composite section)			
		force N_{sI}	stress in steel	force N_s	stress in steel		force		stress	
							N_{sII}	N_{bII}	in steel	in concrete
	cm^2	kN	MPa	kN	MPa	cm^2	kN	kN	MPa	MPa
11	57.4	-187	-32.6	-482	-84.0	108.11	-157	-138	-59.9	-3.1
12	57.4	-331	-57.7	-853	-148.7	108.11	-277	-245	-106.0	-5.4
13	74.0	-432	-58.4	-1113	-150.4	124.71	-404	-277	-113.0	-6.2
14	98.0	-490	-50.0	-1262	-128.7	148.71	-509	-263	-101.9	-5.8
15	98.0	-490	-50.0	-1262	-128.7	148.71	-509	-263	-101.9	-5.8
16	98.0	-476	-48.5	-1225	-125.0	148.71	-494	-255	-98.9	-5.7
17	98.0	-476	-48.5	-1225	-125.0	148.71	-494	-255	-98.9	-5.7
18	74.0	-404	-54.5	-1039	-140.4	124.71	-377	-258	-105.5	-5.7
19	57.4	-288	-50.2	-742	-129.3	108.11	-241	-213	-92.2	-4.7
20	57.4	-130	-22.6	-334	-58.2	108.11	-108	-96	-41.5	-2.1

Area of concrete section - F_b = 450 cm^2, E_b = 25.3·10^3 MPa,
E_a = 2.05·10^5 MPa

Taking into consideration the co-operation between concrete and steel in phase II, that is above the level of assembling load P_m - the stress in steel section, e. c. for the member 13, are reduced from 150.4 to 113.0 MPa, that is nearly 25%. These reduced stresses are "consumed" by the concrete part of the top flange, where the stress in concrete attains a maximum value of 6.2 MPa.

These reduced stresses in steel section in the composite structural model are accompanied by the adequate lower displacement. Deflection charts for considered load levels are shown in Fig. 7.

Taking into consideration the composite structural model, a perfect consistency between the calculation results and geodetic measurements was obtained.
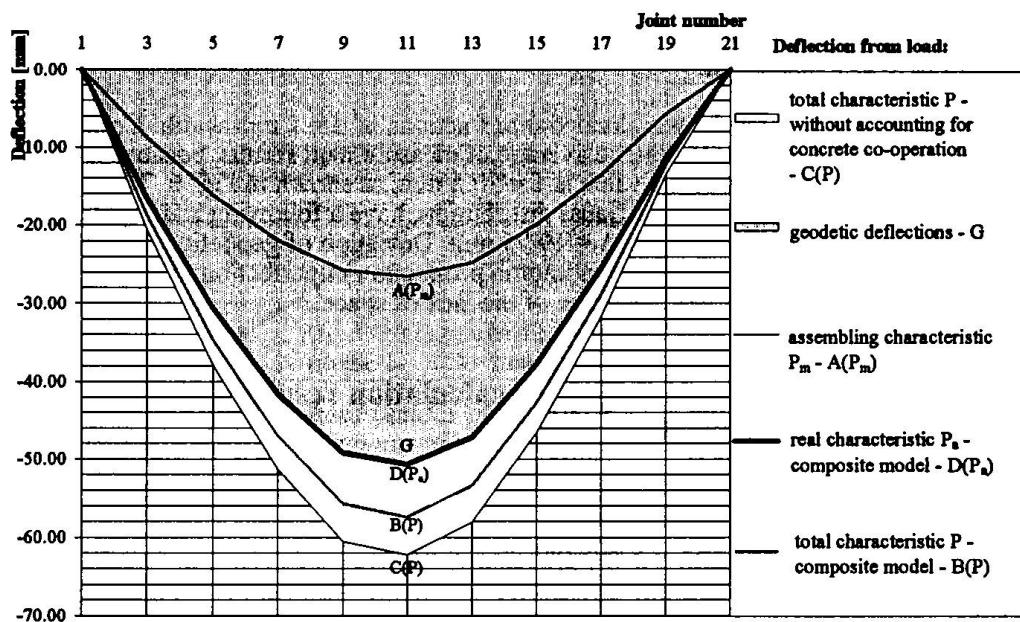

Fig. 7 Calculated and measured displacements of roof girders for considered load levels

In Fig. 7 the points G and $D(P_a)$ coincide, and in Fig. 5, under the real load level P_a, the mean value of the displacement - point G - is obtained.

6. Recapitulation and conclusions

Results of computational static and strength analysis made for the steel roof girders of 30 m span and results of geodetic measurements of vertical displacements of girders' middle joints have been presented in this paper. The latter was treated as an independent second source of information in order to verify the postulate concerning existence of a co-operation between the steel girders' top flange and the concrete curb connected to it.

A classical structural solution of precast thin-walled reinforced concrete slabs supported on upper flange of steel truss girders is the placing of a concrete curb in phase I of construction work. In this phase, i. e. till the load reaches the value of the so-called "assembling" load P_m, the girder works as a "pure" steel truss. In phase II, the concrete curb after hardening and mechanical connection to the girders' top flange, starts work in carrying the load. Girder top flange then works as a composite section, delivering a 16% capacity reserve. The "two-phase" calculation model was positively verified by the geodetic measurements of girder displacement.

The presented example of experimental verification of steel roof girders justifies the formulation of a postulate to introduce the notion of "experimental bearing capacity" into the building codes, so that the research results on deflections and stresses would be equally legalized with the results of static and strength calculations, especially in the case of making a diagnosis of existing structure technical status.

Behavior of Composite Truss Girders

Sheldon L. SHOWALTER
Graduate Research Assistant
Virginia Polytechnic Inst. and State Univ.
Blacksburg, VA, USA

Michelle RAMBO-RODDENBERRY
Via Doctoral Fellow
Virginia Polytechnic Inst. and State Univ.
Blacksburg, VA, USA

W. Samuel EASTERLING
Associate Professor of Civil Eng.
Virginia Polytechnic Inst. and State Univ.
Blacksburg, VA, USA

Thomas M. MURRAY
Montague-Betts Professor of Struct. Steel Design
Virginia Polytechnic Insti. and State Univ.
Blacksburg, VA, USA

Summary

This paper reviews the results of a series of tests that focus on the behavior and strength of composite truss girders. Three laboratory size floors were constructed and loaded to failure. Top chord supported open web trusses were used as secondary members. Three unique methods of generating composite action in truss girders are examined.

1. Introduction

As the use of composite long-span trusses has increased, interest in developing better and more efficient applications of this type of system has also increased. Historically, composite floor design has been applied only to the trusses directly supporting the composite slab. The girders supporting these trusses are usually either non-composite hot-rolled universal beams or non-composite truss girders. As a result, composite truss research has focused only on those trusses which directly support the deck sheeting and concrete.

With the increased use of composite trusses, it is of interest to study the behavior of supporting composite truss girders. A primary consideration in creating a floor system with composite truss girders is the method used to frame the trusses into the truss girders so that the shear studs can be properly attached to the truss girders. Three separate methods of framing were selected for study. Each of these methods is presented and the test results reviewed in this paper.

2. Research Program

A series of three composite floor systems were recently constructed and tested at Virginia Polytechnic Institute and State University. Destructive testing was performed to determine the strength of the girders and observe their behavior within floor systems. These systems included the influence of truss connection behavior on the girders and thus the girder behavior in an actual structure was better approximated.

Each test setup used three full-size girders, spanning 9.1 m and spaced at 2.1 m on center. The setups consisted of an interior truss girder (IG) and two exterior truss girders (EGL, EGR). For the third setup only, a universal beam (EB) was substituted for one of the exterior truss girders to compare the composite action of the two girder types. Secondary trusses, which would generally span from 9 m to 20 m in an actual structure, were shortened for testing to about 2 m and placed between the girders at the third points. Steel sheeting was placed perpendicular to the secondary trusses and parallel to the truss girders. Figure 1 shows the typical framing plan.
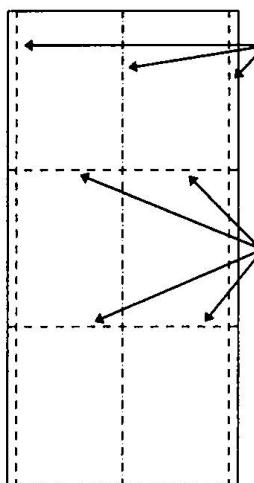

Fig. 1 Test Floor - Plan View

Flush Frame X-section

Stub Girder X-section

Haunch Girder X-section
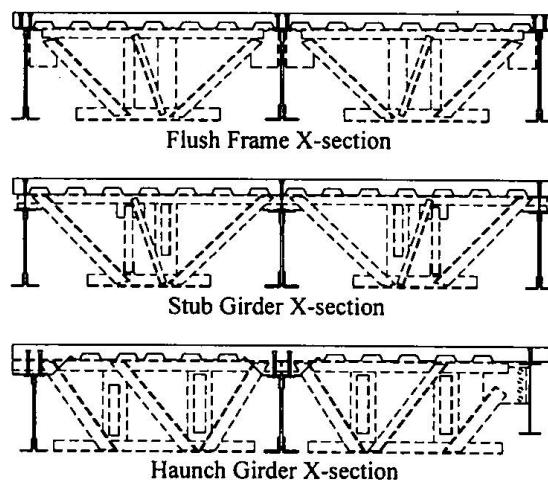
Fig. 2 Specimen Cross-Sections

Headed shear studs were used as the shear connectors; the secondary trusses all had double rows of studs placed in their strong (favorable) positions (Easterling et al 1993). One layer of woven wire fabric was used throughout the entire slab of each setup for temperature and shrinkage effects. Transverse reinforcement was designed separately for each girder in each test setup. The concrete slabs were all constructed of 51 mm steel deck with 76 mm of concrete cover, for a total depth of 127 mm. The girder ends were simply supported by rollers resting on load cells, which were used to measure the girder end reactions.

The systems were loaded with two hydraulic rams which were anchored in load frames and positioned over the secondary trusses. Each ram applied load to a spreader beam which divided the load into two concentrated loads on each secondary truss line. These loads were transmitted by the trusses to the girder third points; the girders then carried the loads to their end supports. The concentrated load points, as well as the rams, could be moved to create different loading situations.

The first setup was a flush framed configuration. The second setup involved the use of stub girders, while the third employed concrete haunches over the girders, as shown in Figure 2. The systems were all tested to observe their composite behavior. Several load applications were performed on each floor. The first application of each test was to load the exterior girders to their predicted service loads and then unload. The load points over the trusses were then repositioned to principally load the interior girder. The second application loaded the interior girder to its predicted service load. The third application loaded the interior girder to 1.67 x service loading, which is the load at which the girder bottom chord would theoretically yield.

The load points were then shifted back to their original positions so that the exterior girders could be loaded to 1.67 x service loading. Further cycles would then be performed with the load points directly over individual girders, as necessary, to load them to failure. During these tests, measurements were taken of strains at various locations along the girders, strains on the surface of the concrete slab, vertical and horizontal displacements of the girders, and slips between the concrete slab and the girder top chords. Detailed descriptions of each of these tests are found in the project reports (Kigudde et al 1996; Showalter et al 1997a, 1997b).

2.1 Flush Framed Tests

For this setup, the secondary trusses were connected to the truss girders with flush-framed, bolted connections. This allowed the top chords of the trusses to be positioned at the same elevation as the top chords of the girders. The steel sheeting could then be placed directly on the top chords of both the girders and the trusses. Shear studs were spaced along the girder lengths to provide sufficient shear resistance to develop the truss girder bottom chord nominal yield stress values. Three-bolt (on EGL) and four-bolt (on EGR) single plate (fin plate) framing connections were used for evaluation purposes.

Eleven different loadings were placed on the system. Symmetric loading patterns were first used to load the girders to their predicted service and first yield strengths. A series of tests were then conducted using unsymmetric loading. Additional symmetrical loads were placed on the system to establish non-linear behavior in the girders, followed by tests to failure of the individual girders.

The exterior girder, EGL, carried a maximum total load (structure dead load + applied load) of 783 kN. The bottom chord was beginning to yield when the girder failed abruptly as a compression web member buckled during a subsequent load application. EGR carried a maximum total load of 776 kN and later failed when a web member buckled. The bottom chord had not reached yield when failure occurred. IG carried a maximum total load of 1535 kN, with definite yielding of the bottom chord. The girder failed completely when compression web members buckled.

2.2 Stub Girder Tests

The second setup utilized a stub girder arrangement, similar to the concept described by Chien and Ritchie (1984), to form the composite truss girders. The secondary truss top chords were seated directly on the girder top chords at the girder span third points. A series of three shallow universal steel beams, or stubs, each approximately 3 m in length, were welded along the length of each girder. The stubs were separated by 200 mm gaps where the secondary truss top chord seats framed in. These stubs filled the 127 mm gaps between the girder top chords and the truss top chords to provide a supporting surface for the steel sheeting. A single row of shear studs was placed directly over the girder centerlines along the girder lengths.

A total of seven loadings were placed on the system. The girders were loaded to their predicted service and first yield strengths, and then the individual girders were tested to failure. Failure in the exterior girder, EGL, occurred in part because of a loss of shear connection at one end of the slab when longitudinal cracking occurred directly along the line of shear studs. Yielding of the bottom chord occurred beneath the third point near the end where the cracks formed. The maximum total load was 670 kN. Similarly, the shear connection on EGR failed when severe

longitudinal cracking occurred along the line of studs on the girder at the opposite end of the setup. It carried a maximum total load of 636 kN. The interior girder, IG, carried a maximum load of 1346 kN and failed as a result of concrete crushing beneath the load points directly over the girder as well as by yielding of the bottom chord at the span third points.

Failure was also caused in part by the formation of plastic hinges in the top chords where the cross-sections were reduced because of the gaps between the stub beams. This introduced higher stresses in the bottom chords at the third points than at midspan, where the girders showed no signs of yielding. The rotation of the slab, occurring as the interior girder deflected, caused several interesting results. Transverse reinforcement had been designed over the girders to resist longitudinal shear. This reinforcement was not sufficient, however, to carry transverse tensile forces in the slab as it rotated. Because of this, the slab cracked longitudinally along the row of studs, causing a loss of shear connection. In addition, as the slab rotated, the secondary trusses rotated as well. The truss seats, being held in place on the girders with welds, caused significant local buckling of the top chord horizontal legs, especially on the exterior girders. This effect would almost certainly be magnified by more typical length trusses.

2.3   Haunched Girder Tests

The third setup used concrete haunches over the girders. As a result, the concrete over the girders was twice the thickness of the normal slab and much longer studs were required. These studs were placed in double rows along the lengths of the girders. The haunches were formed to encase the truss seats. This meant that the seats were cast into the haunch concrete and could be considered additional shear connectors.

This setup also included a universal beam in place of one of the exterior truss girders. The two secondary trusses framing into the beam used four-bolt single plate connections to provide a flush frame on that side of the floor, eliminating the need for a haunch over the beam. A single row of studs were welded directly onto the top flange over the beam centerline. The beam was designed to carry a comparable moment to that of the opposite exterior truss girder (*Load* 1993).

The specimen was subjected to a total of six loadings. The girders were loaded to their predicted service and first yield strengths and then the individual girders were loaded to failure. As in the first setup, no problems were encountered with the strengths of the shear studs on the truss girders. Failure of the beam was a result of a loss of shear connection. It carried a maximum load of 617 kN. The truss girders failed due to yielding of the bottom chords at the span third points. EGL carried a maximum load of 796 kN while IG carried 1845 kN.

3.   Comparison of Predicted and Experimental Results

The ultimate flexural strength of each girder was calculated for the controlling design limit state of bottom chord yielding using measured cross-section and material properties. The ratio of the experimental ultimate moment to calculated ultimate moment, M_e/M_c, for each test is shown in Table 1 and varied from 0.75 to 1.27.

The values of experimental moment of inertia for the specimens were determined from the slope of load vs. deflection curves for the initial loading up to service load. The calculated values were produced by a method incorporating adjustment factors for slip and for the span/depth ratios of the truss girders. The ratios of experimental moment of inertia to calculated effective moment of inertia indicate that the stiffnesses of the flush framed girders and stub girders were accurately predicted. The haunched girders, on the other hand, were much stiffer than predicted.

SETUP	GIRDER	M_e/M_c	I_{effe}/I_{effc}
Flush Framed Girders	EGL	0.93	0.99
	IG	0.99	1.00
	EGR	0.92	1.02
Stub Girders	EGL	0.89	1.01
	IG	0.82	1.01
	EGR	0.86	1.02
Haunched Girders	EGL	1.04	1.10
	IG	1.27	1.30
	EB	0.75	1.02

Table 1   Summary of Composite Joist Girder Tests

The stub girder configuration involved the least labor in terms of shop fabrication of the trusses and truss girders and field erection, but had the poorest performance in terms of strength. The flush framed setup displayed better performance, but it also had greater fabrication demands due to the flush framed connections. The haunched girder setup had the best strength performance, but the field erection was more labor intensive and the slab the most heavily reinforced.

4. Acknowledgments

5. Notation

EB   = Exterior universal Beam
EGL   = Exterior Girder Left (on assigned left of system)
EGR   = Exterior Girder Right (on assigned right of system)
IG   = Interior Girder of system
I_{effe} = experimental effective moment of inertia
I_{effc} = calculated effective moment of inertia
M_e = experimental moment capacity
M_c = calculated moment capacity
P_{max} = experimental maximum total load on a particular girder

6. References

CHIEN, E. Y. L. and RITCHIE, K. L. (1984). *Design and Construction of Composite Floor Systems*, Canadian Institute of Steel Construction.

EASTERLING, W. S., GIBBINGS, D. R. and MURRAY, T. M. (1993). "Strength of Shear Studs in Steel Deck on Composite Beams and Joists," *Engineering Journal*, AISC, 30(2), 44-55.

KIGUDDE, M., RAMBO-RODDENBERRY, M., EASTERLING, W. S. and MURRAY, T. M. (1996). "Flush Framed Composite Joist Girder Tests." *Report No. CE/VPI - ST 96/11.* Virginia Polytechnic Institute and State University, Blacksburg, VA.

Load and Resistance Factor Design Specification for Structural Steel Buildings. (1993). American Institute of Steel Construction. Chicago, Illinois.

SHOWALTER, S. L., RAMBO-RODDENBERRY, M., EASTERLING, W. S. and MURRAY, T. M. (1997a). "Composite Stub Joist Girder Tests," *Report No. CE/VPI - ST 97/02.* Virginia Polytechnic Institute and State University, Blacksburg, VA.

SHOWALTER, S. L., EASTERLING, W. S. and MURRAY, T. M. (1997b). "Composite Haunched Joist Girder Tests." *Report No. CE/VPI - ST 97/03.* Virginia Polytechnic Institute and State University, Blacksburg, VA.

Construction Sequence Effects on
Externally Prestressed Composite Girders

Andrea DALL'ASTA
Dr. Eng.
University of Ancona
Ancona, Italy

Andrea Dall'Asta, born in 1963,
civil engineering degree in 1988
at the University of Ancona, Ph.D.
in 1993. His main research field is
stability and dynamics of externally
prestressed structures.

Luigino DEZI
Professor
University of Ancona
Ancona, Italy

Luigino Dezi, born in 1949,
graduated in civil engineering at
University of Ancona in 1975, professor
of Structural Analysis and Design
since 1994. Research interests include
creep analysis and external prestressing.

Summary

The authors examine composite steel-concrete beams prestressed by external cable, in order to analyze
the influence of the most common construction and prestressing sequences, by evaluating both the initial
linear behavior under service load and the nonlinear behavior under increasing load up to failure. The
analysis is based on a model, described in previous works, which considers the cable slipping at saddle
points and nonlinear constitutive laws for materials composing the structure. In this paper the analysis is
extended for considering different construction sequences in a unitary manner and some numerical
results on simply supported and continuous two-span girders are reported.

1. Introduction

External prestressing, often used in brigde construction and strengthening, usually employes cables
disposed parallel to the steel beam web and anchored at ends. Cable profiles are defined by saddle points
at which they can slip with negligible friction.
Generally, stretched cables permit increasing the global load-carrying capacity, however some other
advantages derive from their presence. At service conditions maximum deflection can be controlled and
notably reduced. In continuous beams concrete deck cracking at intermediate supports can be prevented
under a wide range of external loads. The cables undergo small stress increments under service load
thanks to the redistribution of traction due to slipping and this determines a further ductility resource at
failure.
Substantially different construction and prestressing sequences are adopted in practice [1, 2], leading to
different collapse modalities and different stress and strain distributions in materials (concrete, beam
steel, reinforcement steel and high-strength cable steel). Such differences have not been sufficiently
investigated in the past and this paper intends to show the different behaviors under increasing external
loads up to failure for the following three cases.
Case A. The concrete deck is cast on the steel beam supported by a large number of additional supports
(propped beam). After the concrete hardening the additional supports are removed and prestressing is
applied.
Case B. The concrete deck is cast on the steel beam supported by the final constraints only (unpropped
beam). After concrete hardening prestressing is applied.
Case C. Prestressing is applied to the steel beam only, before the concrete deck cast.
In all the previous cases the concrete deck can be separately prestressed before the connection with the
lower steel beam, obtaining a further increment of compressive stress to prevent cracking.

In previous works [3, 4], the authors presented an analytical model and a numerical solving procedure which consider the nonlinear consitutive behavior of materials and the slipping of the cable at saddle points.

In this paper analytical and numerical aspects are briefly recalled and attention is focused on construction sequences, by defining a unitary approach and by showing some results of practical interest.

2. Nonlinear analysis for different construction sequences

The model of beam displacements preserves the cross section planarity and the orthogonality with the deformed axis, so that the beam strain $\varepsilon_b(x, y)$ can be deduced from the axis displacements in the longitudinal direction $u_0(x)$ and the axis deflection $v_0(x)$, in the following form

$$\varepsilon_b = u_0' - y v_0'' \tag{1}$$

The cable strain derives from the deformation of the whole beam. Denoting by the vector Q_i with components (x_i, y_i), the initial positions of the intermediate saddle points (i=1..D-1) and anchorages (i=0, i=D), and denoting by $\Delta_i(\varphi)$ the difference of the values assumed by a generic function φ between the saddle points i and i-1, the cable strain assumes the following expression

$$\varepsilon_c(u_{0i}, v_{0i}, v_{0i}') = \frac{1}{\Lambda} \sum_{i=1}^{i=D} \alpha_i \left[\Delta_i(u_0) - \Delta_i(y v_0') \right] + \beta_i \Delta_i(v_0) \tag{2}$$

where $\Lambda = \sum_{i=1}^{i=D} |Q_i - Q_{i-1}|$ is the cable length in the reference configuration; α_i and β_i are geometrical terms related to the cable profile. The expression is linearized coherently with the assumption of small displacements and rotations. The nonlinear elastic constitutive laws of beam materials and cable can be posed in the form:

$$\sigma = F(\varepsilon - \varepsilon_0) \tag{3}$$

where ε_0 is the residual strain present at the reference configuration.

The equilibrium condition is determined by means of the Virtual Work Principle. The numerical solution of the nonlinear problem has been performed by approximating the diplacement fields with shape functions and solving the system of equilibrium equations by using the iterative Newton-Raphson method, [3, 4].

The nonlinear analysis prevents superimposing stresses at every construction step, nevertheless the analysis remains sufficiently simple by identifying the correct residual strain to consider at each construction stage. In the sequel the configuration at which the stress is null at all the points of the steel beam, which is present at each construction stage, is assumed as the reference configuration. So that, in all the anlyses the following condition is considered

$$\varepsilon_0 = 0 \quad \text{in steel beam.}$$

The residual strains in concrete deck, reinforcements and cable must be determined in each stage of the different construction sequences.

Case A - propped beam prestressed after the concrete deck cast

The case of propped beam is the simplest situation because no preventive analysis is required for evaluating the nonlinear behavior under increasing loads. In the case of cast in situ concrete deck, the

residual strain is null in the whole beam while the residual strain in the cable ε_{0p} permits controlling the prestressing traction force. The effects due to a preventive prestressing applied to the upper concrete deck before the connection with the steel beam can be analyzed by introducing a residual negative strain ε_{0pc} furnishing the suitable compressive stress in the concrete slab prestressed separately. In conclusion, the following residual strains must be adopted in the analysis:

$$\varepsilon_0 = 0 \quad \text{or} \quad \varepsilon_0 = -\varepsilon_{0pc} \qquad \text{in the deck concrete and reinforcements;}$$
$$\varepsilon_0 = -\varepsilon_{0p} \qquad\qquad\qquad\qquad \text{in the cable}$$

Case B - unpropped beam prestressed after the concrete deck cast

The case of unpropped beam prestressed after the deck cast requires an initial analysis describing the behavior in the initial stage where the sole steel beam undergoes weight loads of both steel beam and concrete deck. This preventive analysis also permits evaluating the axis displacements $\bar{u}_0$ and $\bar{v}_0$ required for determining the residual strain to be considered in reinforced concrete deck for the analysis of the second stage where the whole beam (deck, steel beam and cable) is present and where prestressing can be introduced by means of an adequate value ε_{0p} of residual strain in the cable. If the concrete deck is prestressed separately before connection a further residual strain ε_{0pc} must be adopted, as already discussed in case A. In conclusion, in the analysis of the second stage the following residual strain fields have to be considered.

$$\varepsilon_0 = \bar{u}_0' - y\bar{v}_0'' \quad \text{or} \quad \varepsilon_0 = \bar{u}_0' - y\bar{v}_0'' - \varepsilon_{0pc} \qquad \text{in the deck concrete and reinforcements;}$$
$$\varepsilon_0 = -\varepsilon_{0p} \qquad\qquad\qquad\qquad \text{in the cable}$$

Case C - beam prestressed before the concrete deck cast

The case of unpropped beams prestressed before the concrete deck cast, differs from the previous case only because in the preventive analysis describing the structural behavior at the first construction stage, the cable is present and the prestressing force is applied by means of ε_{0p}. Once the displacement fields $\bar{u}_0$ and $\bar{v}_0$ existing in the first stage are determined, the residual strain field to be considered for the upper deck in the second construction stage is furnished by an expression formally equal to that adopted in case B, even if the axis displacements $\bar{u}_0$ and $\bar{v}_0$ are different. Separately prestressing of the concrete deck can be taken into account as in previous cases.

3. Applications

The applications consider composite beams with depth H=1870mm and with the cross-section described in detail in Fig.1.
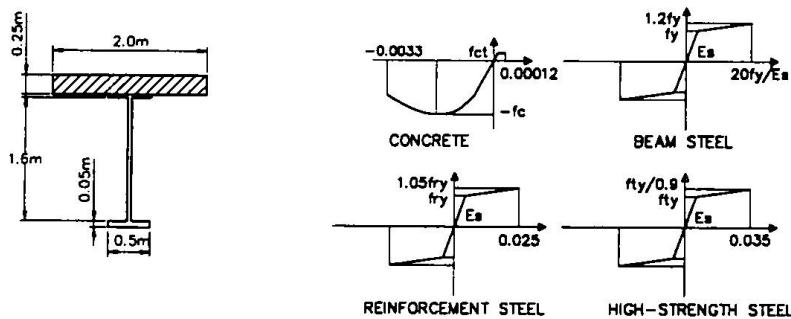

Fig.1 Composite cross section and constituive laws.

The concrete has a cylindrical compressive strength fc=33 MPa, tensile strength fct=2.5MPa and analyses were performed by using the constitutive law proposed in EC2 [5] (see Fig.1).Steel behavior was been modeled by means of a bilinear curve defined by elastic modulus, yield stress, failure stress and failure strain (see Fig.1). Beam and reinforcement steel have an elastic modulus Es=210 GPa while cable steel elastic modulus is Es=190 GPa. The yielding stress of beam, reinforcement and cable steel are respectively fy=280 MPa, fry=440 MPa, fty=1680 MPa.

The following applications analyze the influences of the three construction sequences by comparing the deformation and stress progress under increasing loads up to failure.

Simply supported beam

The results refer to a simply supported beam with span L=30 H, prestressed by a tendon anchored at the centroids of the end cross section and draped along a profile defined by two intermediate saddle points. In case A and B the tendon is anchored at the centroid of the composite section while in case C it is anchored at the centroid of the steel beam. The initial prestressing force is equal to 5000 kN and stress is equal to 1000 MPa in all the cases.

Fig.2 shows the load-midspan deflection curves for the three cases A, B, and C, while Fig.3 describe the maximum stress progress respectively in concrete and steel. It can be noted that the ultimate loads are almost the same in all the cases thanks to stress redistribution due to plasticity of materials while more

large differences can be observed on displacements and stress distributions (Fig.2). In case B the deformation due to prestressing, applied to the complete section, approximatively balances the deformation due to dead loads, applied to the steel beam only, while in case A midspan displacements are usually positive under service loads. Case C differs from case B only because prestressing acts on the more deformable steel beam, even if large differences do not occur because the cable eccentricity is smaller in case C.
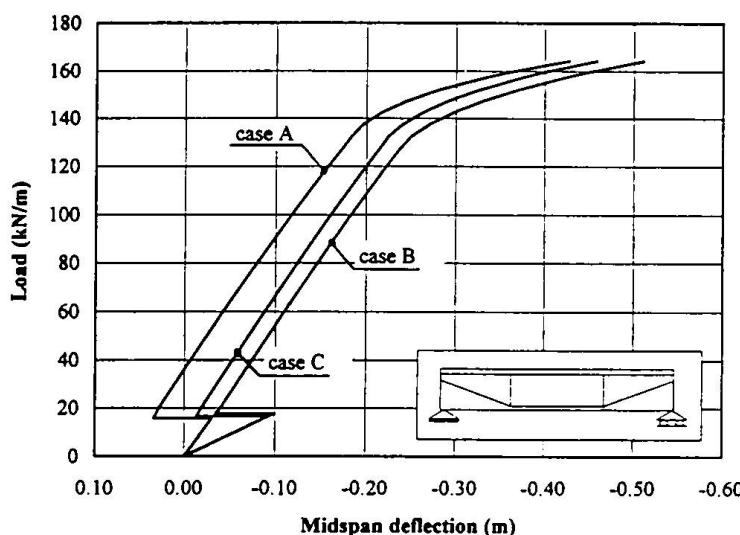
Fig.2 Midspan displacement versus load for sequences A, B, C.
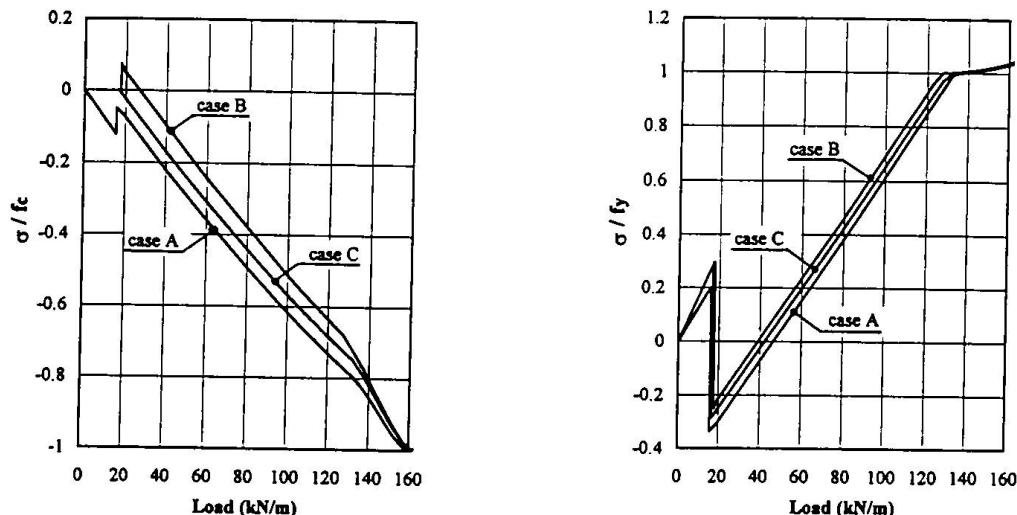

Fig.3 Progress of maximum stress in concrete (a) and steel (b).

In the three cases the stiffness progress is similar: it remains approximatively constant for a large load range and drastically reduces when the lower steel flange yields (Fig.3). In the considered cases, concrete reaches its maximum stress for a slightly larger load (Fig.3). Cable does not fail thanks to stress redistribution due to slipping even if it equally undergoes notably stress increment.

In the case A and B the prestressing force level is conditioned by upper deck cracking under dead loads while no problem exists in case C where concrete is surely compressed under dead loads, so that this latter seems to be the most effective construction sequence under the point of view of cracking prevention. Other phenomena not considered here, such as shrinkage, may contribute to increasing deck cracking.

Two-span continuous beam

A two-span continuous beam with span L=35H and a cable draped by three saddle points, one located at the intermediate support and two at the span sections with maximum moment under uniform load is considered. The lower steel flange has been enlarged in the negative moment region (thickness 120mm) so that the midspan section and support section approximatively reaches ultimate strains at the same load level. The prestressing force is equal to 7000 kN and the cable is anchored at composite cross-section centroids in case A and B and at steel beam centroids in case C. Fig.4 shows the curve load-deflection at the section where saddle points are located, Fig.5 reports the progress of concrete and steel maximum stress in the spans, Fig.6 shows the progress of maximum stress in concrete, reinforcement and the beam lower flange at the support section.
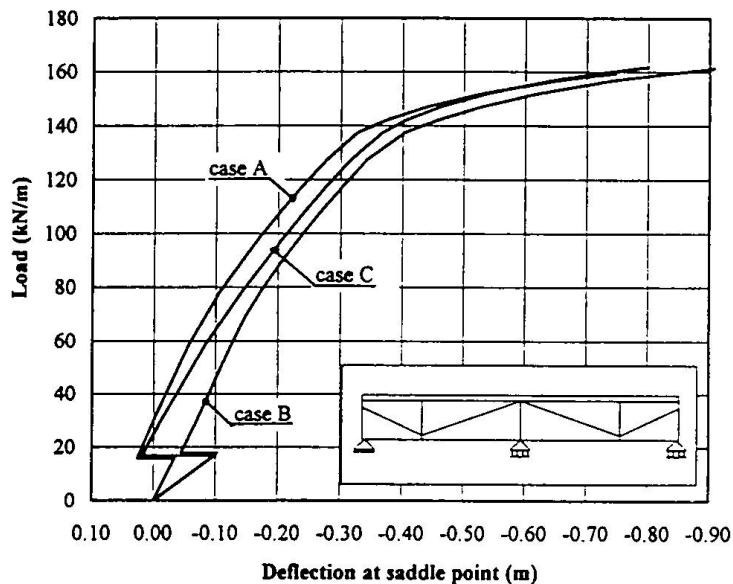

Fig.4 Midspan displacement versus load for sequences A, B, C.
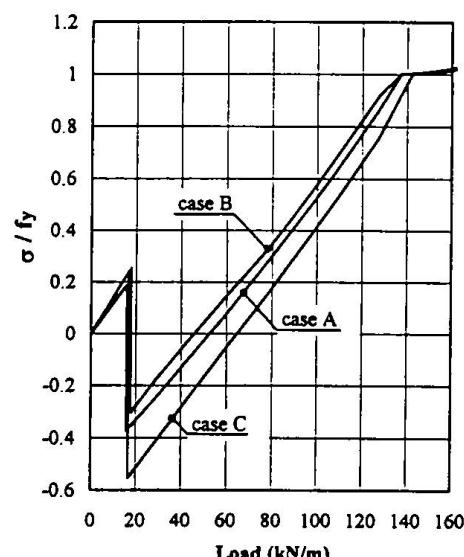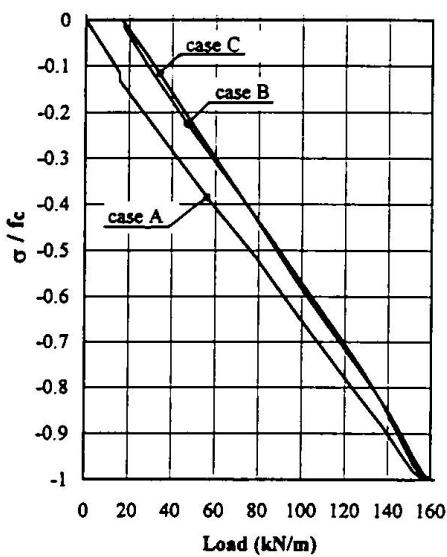
Fig.5 Midspan section: progress of maximum stress in concrete and steel.

This structural system exibhits a more complex behavior: in this case larger differences occur between displacements deriving from prestressing on the whole beam (cases A and B) and prestressing acting on the sole steel beam (case C); case C shows a lower global stiffness for a large load fields, mainly caused by concrete traction failure; steel however yields for higher loads in case C and the global stiffness achieves similar value for all the cases in the last phase. The support section attains yielding for a lower load level with respect to span section and, even in this case, plasticity of materials leads to small differences in the ultimate carrying load capacity in the three cases. The smallest deflections at low load level are observed for cases A and C while the largest deflections occur in the case B.

In the considered beam, yielding of steel precedes the concrete failure at spans (Fig.5). The stress progress in concrete are almost similar in case B and C while a higher compressive level can be observed in case A. Prestressing however has little effectiveness on concrete at span section. A noticeable reduction of tensile stress exists in the three cases and yielding occurs at higher load level in the steel beam of case C thanks to the prestressing modalities.

In continuous beams prestressing permits a sensible reduction of cracking in the region with negative moment, even if the usual prestressing advantages are partially limited by the positioning of saddle points parallel to the web that does not permit obtaining large eccentricity.

In particular, it is evident from Fig.6 that in cases A and B cracking is prevented for a large range on external loads while, contrary to the previous case of simply supported beams, no advantages can be obtained in case C. The stress progress in reinforcement rapidly increases after the deck craking in cases A and B while in case C reinforcement yields for a much lower load level (Fig.6). Prestressing shows a little effectiveness in case C while a significative reduction of compressive stress occurs in case A and B.
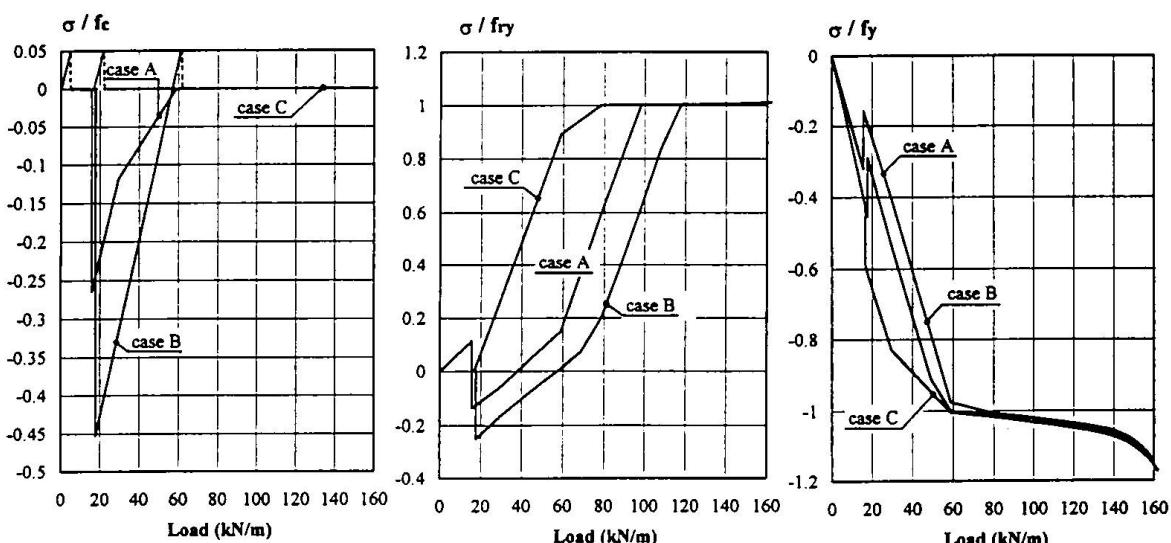

Fig.6 Section at support: progress of maximum stress in concrete, reiforcements and beam steel.

4. References

1 Saadatmanesh H., Albrecht P., Ayyub B.M. (1989). Guidelines for flexural design of prestressed composite beams. *J. Struct. Engrg., ASCE,* 115(11), 2944-2961.

2 Ayyub B.M., Sohn Y.G., Saadatmanesh H, (1992), Prestressed composite girders. II: Analytical study of negative moment. *J. Struct. Engrg., ASCE,* 118(10), 2763-2783.

3 Dall'Asta A., Dezi L. (1993). Nonlinear analysis of beams prestressed by unbonded cables. *J. Engrg. Mech., ASCE,* 116(11), 2931-2951.

4 Dall'Asta A., Dezi L. (1997). Non-linear behavior of externally prestressed composite beams: analytical model. Submitted for publication.

5 "Eurocode No.2: Design of concrete structures" (1991). Eurocode 2 Editorial Group.

Behaviour of Composite Box Girder Sections at Ultimate Limit State

Hugo CORRES PEIRETTI
Prof. Dr.
E.T.S.I. Caminos, Canales y Puertos
Madrid, Spain

Jorge CALVO BENITEZ
Civil Engineer
E.T.S.I. Caminos, Canales y Puertos
Madrid, Spain

Summary

In this paper the method proposed by RPX-95[1] for the analysis of the behaviour of composite cross-sections subject to normal forces is briefly explained. This procedure allows the modelling of the behaviour in Ultimate Limit State, as well as in previous strain situations (moment-curvature diagram). An experimental program designed to test this approach, and presently under way, is also presented, as well as some of the results obtained so far.

1. Introduction

Eurocode 4 [2] as well as other standards [3,4] propose different approaches for the analysis of the bearing capacity of composite cross-sections subject to normal forces (Elastic, Corrected Elastic, Plastic, Elasto-Plastic). The Elasto-Plastic method, which models the behaviour in the most realistic manner, is formulated for slender compressed plates and stiffened compressed plates in terms of stresses. This fact does not permit the determination of the corresponding strain, and therefore does not allow to evaluate the ductility available.

The recently published RPX-95 'Recommendations for the Design of Composite Highway Bridges' [1] includes a different elasto-plastic approach for the evaluation of the Ultimate Bearing Capacity (Ultimate Limit State) and for the evaluation of intermediate strain states (Moment-Curvature diagram). The main aspects of this procedure are discussed in what follows. This procedure allows to determine the deformational state of the cross section for every load level.

In order to test this procedure, an experimental program, which is briefly presented in this article, is being carried out. Some of the results obtained so far are also presented.

2. Sectional Behaviour

The study of composite cross-sections subject to normal forces requires the use of models which adequately represent the behaviour of slender compressed plates, stiffened compressed plates, slender plates stiffened by conection to a concrete slab (double composite action), etc. This subject has been extensively studied in the past few years [5] [6] [7]. The models developped, however, are formulated in terms of stresses, which makes their use difficult, since, when dealing with non-linear behaviour, the most adequate approach is the formulation in terms of strains.

The recently published RPX.95 'Recommendations for the Design of Composite Highway Bridges' [1] establishes a model which allows the representation of the behaviour of slender plates in terms of strain. This model has been developed on the basis of the classical method of efective widths [5], taking into account the tests and research carried out by several authors [8] [9][10] (fig. 1).
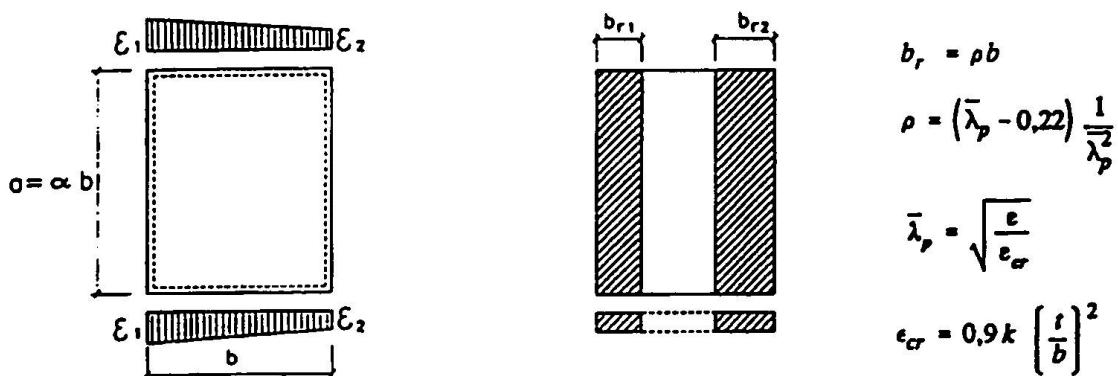

Figure 1. Model for slender compressed plates.

For stiffened compressed plates, the model takes into account the instability of the both of the plate between stiffeners and the stiffener and the plate acting together (fig. 2).

1   Elastic behaviour
2   Plate buckling and/or stiffener buckling
3,4   Stiffener buckling and/or plate buckling
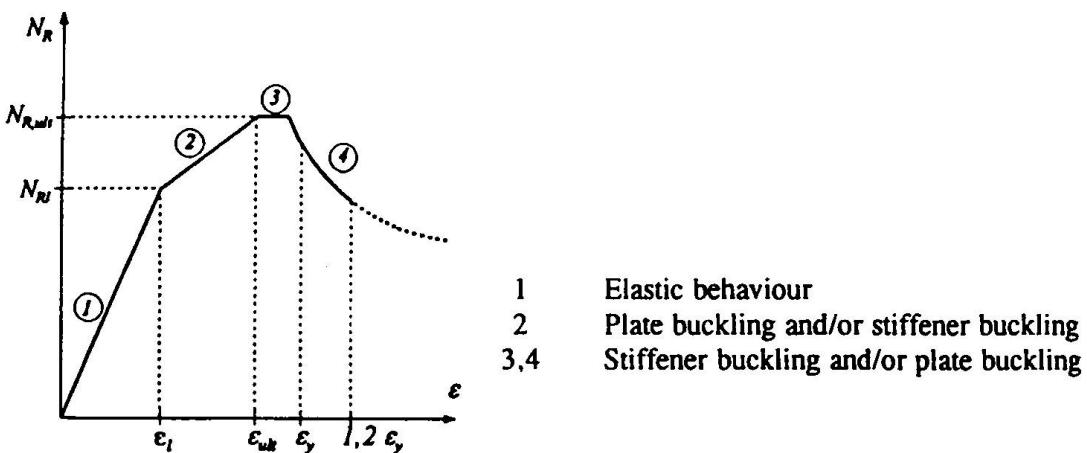
Figure 2. Model for stiffened compressed plate. RPX-95.

Finally, RPX-95 [1], following a similar method used in concrete structures for a long time, establishes a criterium in order to characterize the ultimate capacity of a cross section (fig 3). For this the ultimate strain of different fibres is assumed.
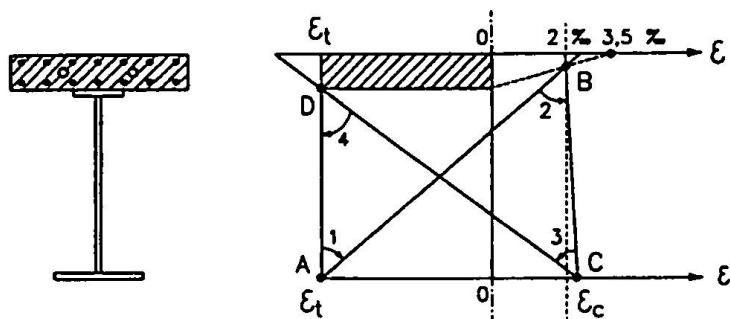
Figure 3. Ultimate strain conditions for Ultimate Limite State due to normal forces.

3. Experimental Program

3.1. Specimen description.

The experimental program includes four beams consisting, each one, in a span of 6600 mm and a cantilever of 2475 mm of length. In each test, the cantilever is initially loaded until failure of the support cross-section. Then, the main span is tested, also until failure of the most stressed cross-section.The beams are equipped with transverse diafragms over the supports and also with transverse stiffeners on the webs every 825 mm.
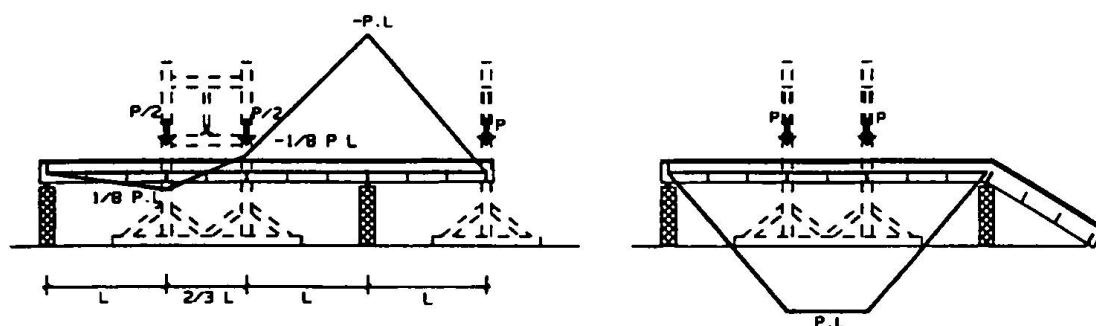

Figure 4. Test layout. Left: negative moments at support. Right: positive at center span.

The characteristics of the materials used for the beams are included in table 1.

Concrete		Steel		
Top slab	Bottom slab	Reinforcement	Plates	Stiffeners
C25	C25	Grade 500	S 355	S 275

Table 1. Nominal values of the materials used for the tests.

The geometry of the different critical cross-sections in the tested beams is shown in figure 5.

The sections are representative of the most widely used typologies for composite box girders in Spain (lower plate stiffened in the negative bending region with concrete, plates with different types of stiffening systems), and of the different structural behaviours.
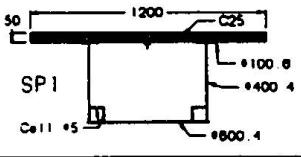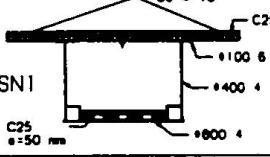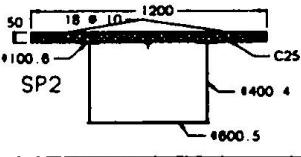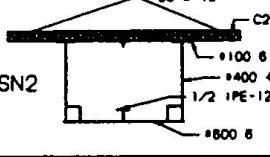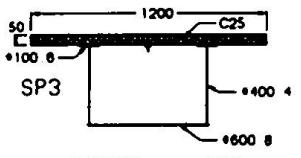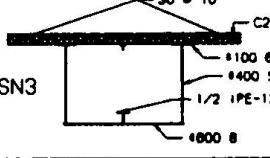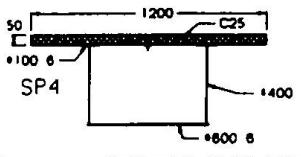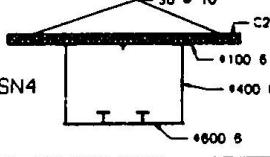
Figure 5. Geometry of the critical cross sections.

In order to take into account the construction procedures most frequently used, beams VMX2 and VMX3, on one hand, simulate unshored construction. Experimentaly, this situations is simulated by loading the structure before concreting the top slab (see photograph 1). Beams VMX1 and VMX4, which, on the other hand, simulate the case of shored construction, the top slab is concreted with the steel beam supported at intermediate points between the final supports.

In figure 6, the theoretical moment-curvature diagram, obtained according to the criteria presented in paragraph 2 for the cross sections at the center of the main span and at the support is shown.
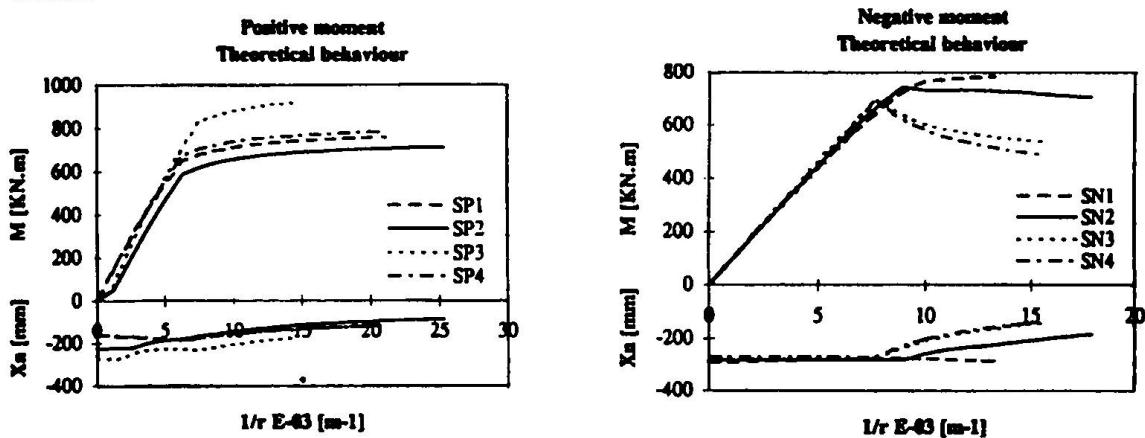

Figure 6. Theoretical moment-curvature diagrams for the critical cross sections.

3.2 Beam monitoring system

The monitoring system of the tested beams consists of:

- Load cells. In order to control both applied load and the reactions of the structure.
- Strain gauges in order to determine the state of strain at different cross-sections and plates.
- LVDT. The transducers are located on the concrete top slab and provide measurements of mean strains.
- Deflection gauges. They are used to measure global deflections of the cantilever and central span.

All the measurements were controlled and registered by a data adquisition system which allows the visualization in real time of the behaviour of different cross-sections and their comparison to the theoretical results.

4. Experimental results

In photograph 2, a moment of the loading of a center span is shown, after having completed the testing of the cantilever.
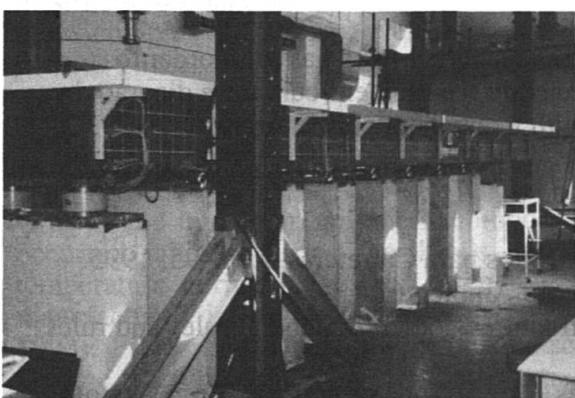
*Photograph 1. Preloading of the steel girder VMX2 before concreting of top slab.*
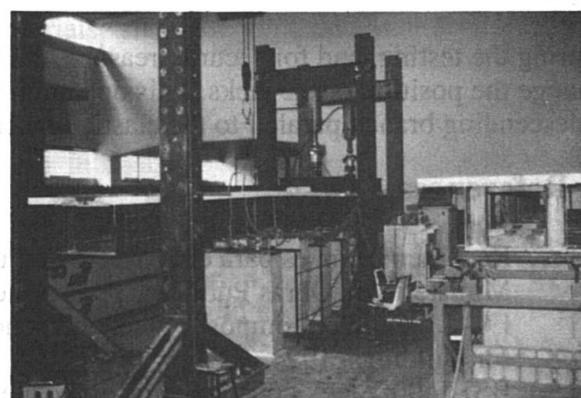
Photograph 2. Testing of center span. Beam VMX2.

In figure 7.1, the theoretical moment-curvature diagram (obtained using the premises described in 2.) for the support cross section of beam VMX2 is compared to the experimental results. In the same figure the evolution of the fibre of zero strain is also shown. As can be seen the experimental results and the theoretical predictions show good agreement.

The first change in stiffness observed coincides with the cracking of the top slab. The second stiffness loss is due to the begining of the buckling of the lower plate. The failure of the cross section finally results from this instability.

In figure 7.2 the moment-curvature diagram and the evolution of the position of the zero strain fibre are shown, both the observed values and the predicted ones, for the center span cross section.The diagram shows the influence of pre-loading. After the concreting, the cross section behaves more or less linearly until the yielding of the structural steel takes place.
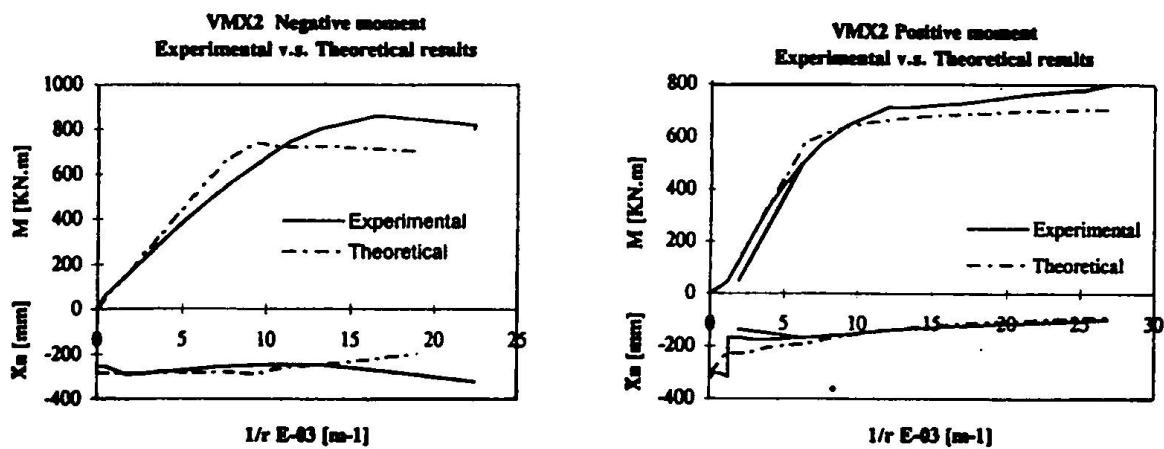
7.1 Support cross section   7.2 Center span cross section

Figure 7. Moment-curvature diagrams. Experimental v.s. theoretical results.

The measurements were halted when the measuring range of the monitoring devices was surpassed, however, the load process continued until failure of the beam was reached with a great deflection at center span.

As can be seen the position of the zero strain fibre is always high, so that almost all the steel cross-section is in tension. With the yielding of the steel, the position of this fibre becomes even higher.

During the testing, and for security reasons, the loading process had to be halted in order to change the position of the jacks. This operation is reflected in the moment-curvature diagram by a descending branch paralell to the elastic branch but with a remanent plastic strain.

5. References

[1]   Recomendaciones para el Proyecto de Puentes Mixtos para Carreteras. RPX-95, 1995. Ministerio de Obras Públicas, Transportes y Medio Ambiente.
[2]   EC-4.Design of composite steel and concrete structures. Part 1-1. General rules and rules for buildings. 1994
[3]   BSI 5400. Steel, concrete and composite bridges. Part 5. Code of practice for design of composite bridges.1979.
[4]   SIA 161. Constructions métalliques. 1990.
[5]   P. Dubas; E. Gehri. Behaviour and design of steel plated structures. ECCS. CECM. EKS. 1986.
[6]   European Recommendations for the design of longitudinal stiffened webs and of stiffened compresion flanges. Nª 60. ECCS. CECM. EKS. 1990.
[7]   W. Hindi; J.E. Harding. Recommendations for the design of stiffened girder flanges under uniaxial compression. Bridge Assesment Management and design. Elsevier Science. 1994.
[8]   K. Ghavami. Experimental study of stiffened plates in compression up to collapse. J. Const. Steel Research. Elsevier Science. 1993.
[9]   Vayas, I.; Psycharis, I. Dehnungsorientierte Formulierung der Mehode der wirksamen Breite. Stahlbau, 61 (1992).
[10] Calvo, J.;Corres, H. Propuesta de ensayos de secciones mixtas en cajón en E.L.U. Informe anual. E.T.S.I. Caminos,Canales y Puertos de Madrid. 1994.